

A TRIDENT SCHOLAR PROJECT REPORT

NO. 262

INCORPORATION OF A MAGNETOTAIL INTO THE MODEL OF THE
GLOBAL SATURNIAN MAGNETOSPHERE



UNITED STATES NAVAL ACADEMY
ANNAPOLIS, MARYLAND

This document has been approved for public
release and sale; its distribution is unlimited.

20000424 153

| REPORT DOCUMENTATION PAGE | | | Form Approved OMB No. 074-0188 | |
|--|--|---|-----------------------------------|--|
| Public reporting burden for this collection of information is estimated to average 1 hour per response, including g the time for reviewing instructions, searching existing data sources, gathering and maintaining the data needed, and completing and reviewing the collection of information. Send comments regarding this burden estimate or any other aspect of the collection of information, including suggestions for reducing this burden to Washington Headquarters Services, Directorate for Information Operations and Reports, 1215 Jefferson Davis Highway, Suite 1204, Arlington, VA 22202-4302, and to the Office of Management and Budget, Paperwork Reduction Project (0704-0188), Washington, DC 20503. | | | | |
| 1. AGENCY USE ONLY (Leave blank) | 2. REPORT DATE 4 May 1999 | 3. REPORT TYPE AND DATE COVERED | | |
| 4. TITLE AND SUBTITLE Incorporation of a magnetotail into the model of the global Saturnian magnetosphere | | 5. FUNDING NUMBERS | | |
| 6. AUTHOR(S) Bruch, Jeremy J. | | | | |
| 7. PERFORMING ORGANIZATION NAME(S) AND ADDRESS(ES) U.S. Naval Academy Annapolis, MD | | 8. PERFORMING ORGANIZATION REPORT NUMBER USNA Trident Scholar project report no. 262 (1999) | | |
| 9. SPONSORING/MONITORING AGENCY NAME(S) AND ADDRESS(ES) | | 10. SPONSORING/MONITORING AGENCY REPORT NUMBER | | |
| 11. SUPPLEMENTARY NOTES Accepted by the U.S. Trident Scholar Committee | | | | |
| 12a. DISTRIBUTION/AVAILABILITY STATEMENT This document has been approved for public release; its distribution is UNLIMITED. | | | 12b. DISTRIBUTION CODE | |
| 13. ABSTRACT: An extension to the current Saturnian magnetosphere model can be developed by adding a realistic magnetotail, which thus far the previous models have lacked. The magnetotail structure provides a mechanism for the rejoining of deflected solar wind particles after they have traveled past the planet, following deflection from their original paths as a result of interaction with the magnetospheric field. These particles generate a dawn-to-duskward cross-current as they re-merge to eventually form a neutral plasma streaming outwards. The cross-tail current sheet and its associated return currents generates a magnetotail magnetic field, which provides an additional contribution to the Saturnian magnetospheric field. The incorporation of a magnetotail into Saturn's magnetosphere is predicted to enhance the range wherein the model is applicable on the night side of the planet. This paper incorporates a magnetotail into the currently accepted global Saturnian magnetospheric model and compares the results with Voyager spacecraft data for verification. This new model will be helpful for the Cassini mission when it arrives in 2004 since the satellite will be spending a large fraction of its time at high Saturnian latitudes as Cassini executes its polar orbits. | | | | |
| 14. SUBJECT TERMS Magnetosphere, Magnetopause, Magnetotail, Saturn, Cassini | | 15. NUMBER OF PAGES | | |
| | | 16. PRICE CODE | | |
| 17. SECURITY CLASSIFICATION OF REPORT | 18. SECURITY CLASSIFICATION OF THIS PAGE | 19. SECURITY CLASSIFICATION OF ABSTRACT | 20. LIMITATION OF ABSTRACT | |

U.S.N.A. --- Trident Scholar project report; no. 262 (1999)

**INCORPORATION OF A MAGNETOTAIL INTO THE MODEL OF THE
GLOBAL SATURNIAN MAGNETOSPHERE**

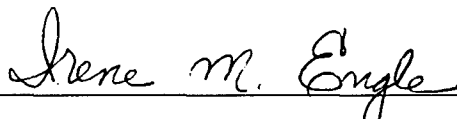
by

Midshipman Jeremy J. Bruch, Class of 1999
United States Naval Academy
Annapolis, Maryland



Certification of Adviser Approval


Professor Irene M. Engle
Department of Physics



4 May, 1999

Acceptance for the Trident Scholar Committee

Professor Joyce E. Shade
Chair, Trident Scholar Committee



4 May 1999

USNA-1531-2

Abstract:

An extension to the current Saturnian magnetosphere model can be developed by adding a realistic magnetotail, which thus far the previous models have lacked. The magnetotail structure provides a mechanism for the rejoining of deflected solar wind particles after they have traveled past the planet, following deflection from their original paths as a result of interaction with the magnetospheric field. These particles generate a dawn-to-duskward cross-current as they re-merge to eventually form a neutral plasma streaming outwards. The cross-tail current sheet and its associated return currents generates a magnetotail magnetic field, which provides an additional contribution to the Saturnian magnetospheric field. The incorporation of a magnetotail into Saturn's magnetosphere is predicted to enhance the range wherein the model is applicable on the on the night side of the planet. This paper incorporates a magnetotail into the currently accepted global Saturnian magnetospheric model and compares the results with Voyager spacecraft data for verification. This new model will be helpful for the Cassini mission when it arrives in 2004 since the satellite will be spending a large fraction of its time at high Saturnian latitudes as Cassini executes its polar orbits.

Keywords: Magnetosphere, Magnetopause, Magnetotail, Saturn, Cassini.

Acknowledgments:

I would like to express my appreciation to the following persons:

My advisor, Professor Irene Engle, for her patience and effort in assisting me with this project.

The Trident Scholar Committee for supporting my efforts in the project.

Karen Lambert and Christine Jamison of the Educational Resources Center (ERC) for helping prepare my poster and oral presentation.

Christopher Rapin for enabling me to obtain the Interactive Data Language graphing codes.

Table of Contents

| | |
|---|----|
| Abstract | 1 |
| Acknowledgments | 2 |
| Table of Contents | 3 |
| I. Introduction | 4 |
| II. Background | 5 |
| A. The dipole field | 5 |
| B. The ring current | 7 |
| C. Determination of the shape of the magnetopause magnetic field | 10 |
| 1. Newtonian solar wind pressure | 12 |
| 2. Magnetic pressure | 14 |
| 3. Pressure balance | 14 |
| D. Magnetotail contribution | 15 |
| III. Method of generating a self consistent model | 25 |
| IV. Observations of a self-consistent idealized global Saturnian model | 28 |
| V. Validation of the Idealized Global Saturnian Model | 32 |
| VI. Non-idealized (Tilted Model) | 35 |
| A. Effects of the non-zero λ_{SW} on the magnetotail | 37 |
| B. Effects of the non-zero λ_{SW} on the magnetopause current elements | 38 |
| VII. Discussion and Conclusion | 40 |
| Bibliography | 41 |
| Appendix A. | 43 |
| Appendix B. | 45 |
| Appendix C. | 46 |

I. Introduction

The purpose of this paper is to present a method of incorporating a magnetotail model into the currently accepted and validated model of the Saturnian magnetosphere. The current models will hereafter be designated as MEBS96 for the 1996 paper written by Sylvestre Maurice, Irene Engle, Michel Blanc and Mark Skubis or ME95 for the 1995 paper written by Sylvestre Maurice and Irene Engle. The advantage of the inclusion of a magnetotail current system into the ME95 and MEBS96 models is its relevance to the Space Physics community as the Cassini Probe approaches Saturn to arrive in 2004. This new model will refine the magnetic field configuration and extend its range of validity on the night side of the planet. Consequently, it should help in the prediction and understanding of observed magnetometer and plasma flow results obtained in the night region of the planet as Cassini orbits *in situ* around Saturn.

The model of the Saturnian magnetosphere (the magnetic field region around a planet), in the past, consisted of three contributions. The first is an approximated intrinsic internal dipole centered in the planet, \vec{B}_D , which is most likely generated via dynamo effects within the planet [Acuna *et al.*, 1981]. However, in general, a multipole expansion is more applicable to the intrinsic field of a planet due to the necessity to account for misalignment between the moment of the field and the rotation of the planet (as is the case for Jupiter) or due to the off center origin of the moment. Fortunately, there is sufficient evidence that the moment of the magnetic field for Saturn is located in the center of the planet and oriented within approximately 1° alignment with the rotation axis of Saturn. Consequently, a pure dipole provides a reasonably accurate fit near the planet.

The second contribution, an azimuthally-rotating equatorial ring current, is also internal to the magnetosphere. This ring current was hypothesized as a means to generate a magnetic field, \vec{B}_{RC} , which deforms the dipole field environment by extending the dipole fields lines associated with a particular latitude origin on the planet in order to obtain better fits to satellite data. As a result, the field lines extend radially outward near the equatorial plane for a given co-latitude starting point in contrast to the field lines resulting from just the dipole contribution.

The final contribution to the currently accepted model is the magnetic field resulting from the magnetopause surface currents, \vec{B}_{SC} , which are generated by the interaction of the solar wind with the internal magnetic field contributions of Saturn. If just the dipole and ring current magnetic field contributions were considered, the

magnetic field of Saturn would extend to infinity. With the inclusion of the solar wind interaction, the net shape of the magnetic field around the planet is confined to a discontinuous boundary called a magnetopause. The surrounding confined region of magnetic field is called the magnetosphere.

Satellite data [Smith *et al.*, 1980] suggest that a magnetotail current system leads to a fourth contribution, \vec{B}_{tail} , to the net magnetosphere of Saturn. Numerous models have been provided to model the Earth magnetotail system. Most of them assume crude approximations or are only applicable over a limited range on the night side of the planet. The purpose of this paper is to take one of the more realistic and sophisticated Earth magnetotail models as published by David Beard in 1979 and adapt it as an incorporation to the ME95 and MEBS96 models. The incorporation of a magnetotail into the Saturnian magnetosphere is predicted to provide significant refinements to the net magnetic field and shape on the night side as well as small alterations to the magnetic field on the day-side. Due to the dominating effects of the solar wind interaction with the magnetosphere on the day-side, it is predicted that the changes of the shape on the day-side of the magnetosphere will be relatively small.

II. Background - Modeling of the first three contributions of the Saturnian magnetosphere

A. The dipole field

As discussed above, the first contribution to the magnetosphere is the pure dipole. It might be useful to understand how the equation for a pure dipole is derived from the basic principles of electricity and magnetism. The bulk of the mathematics in the derivation of a pure dipole magnetic field are shown in Appendix A [Griffiths, 1989]. The resulting dipole equation is

$$\vec{B}_{\text{dipole}} = \vec{\nabla} \times \vec{A}_{\text{dipole}} = \frac{\mu_0}{4\pi r^3} m [(2\cos \theta)\hat{r} + (\sin \theta)\hat{\theta}] \quad (1)$$

Based on the Voyager 1 and 2 observations, the moment, m , in equation (1) can be represented in the following approximation, equation (2):

$$\frac{\mu_o m}{4\pi} = 0.21 \pm 0.005 \frac{G}{R_s^3} \quad (2)$$

The units of the moment presented in equation (2) allow calculation of the dipole in Saturnian radii, ($1 R_s = 60,330 \text{ km}$). The resulting dipole field for Saturn is shown in Figure 1.

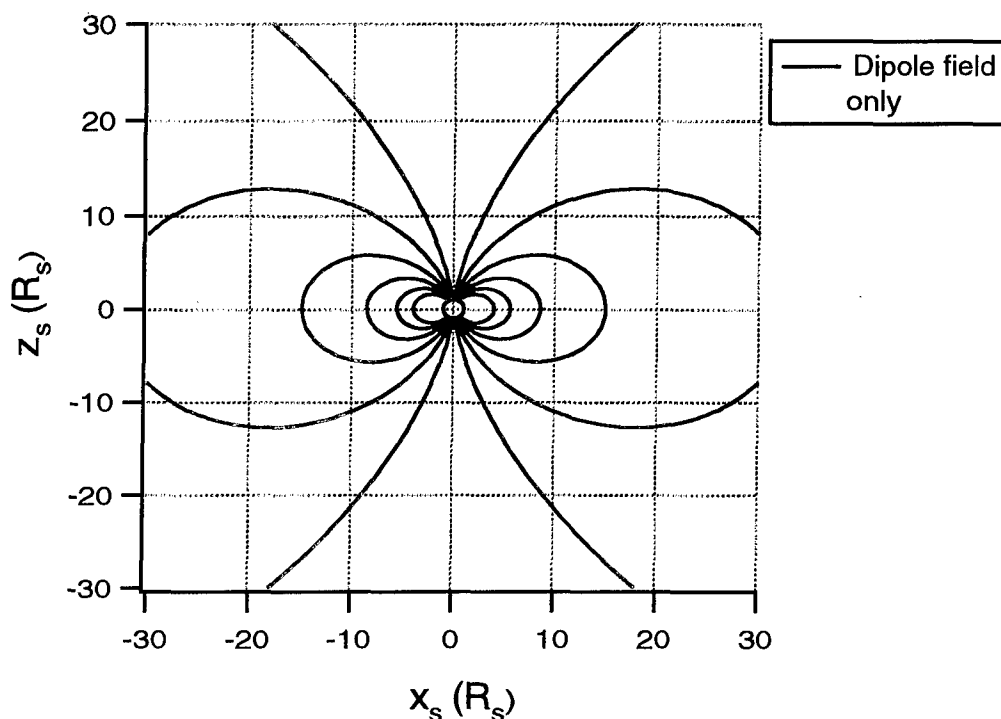


Figure 1. Graph of the Dipole field* of Saturn in the noon-midnight meridian plane (x-z plane). The coordinate system is centered on the planet with the positive x axis pointing towards the sun and the z axis aligned with the magnetic axis. The units in the Figure are measured in Saturnian radii.

*Note: In Figure 1 and in all other graphs of magnetic field lines in this paper, the indicated lines on the graph are always parallel to the magnetic field vector, \vec{B} . In other words, if one picks a point on the magnetic field line, the projection of the magnetic field vector in the plane of the graph can be determined by drawing a tangent to the field line at that point. Only relative magnitudes of net magnetic field values can be determined by looking at the density of field lines in a particular region on the graph. Consequently, a region with a low density of magnetic field lines will have a low net

magnetic field value relative to a region on the graph with a higher density of magnetic field lines.

B. The ring current

It was observed that the magnitude of the net magnetic field measured by Voyager 1 and 2 (V1 and V2) deviates from a pure dipole. The addition of a ring current system composed of an azimuthally axi-symmetric shape was sufficient to account for this deviation in the net magnetic field relative to the pure dipole field shown in Figure 1. The axi-symmetric shape is similar to that of a washer disk with inner radius, a , outer radius, b , and half thickness (the distance from the equatorial plane of Saturn to the top of the disk), D . The orientation of these parameters relative to the Saturnian magnetosphere neighborhood can be seen in the rectangular boxes in Figure 3. The parameters of the ring current were developed in order to fit the V1 and V2 magnetometer data.

The parameters used for the ring current model in this paper are the same as those used in the ME95 model which utilized a refined version of the model developed by Connerney et al. in 1983. The ME95 model accounts for solar wind interaction as well as the intrinsic dipole in determining the parameters for the ring current system. The model developed by Connerney et al., on the other hand, only accounts for the intrinsic planetary dipole field in its determination of the ring current parameters. The radial values of the disk were not adjusted in the ME95 model since they were determined fairly accurately from V1 and V2 plasma data. Observations showed that the plasma current system extends from $a = 8 R_S$ to $b = 15.5 R_S$ centered on the equator. The half thickness, D , was adjusted in the ME95 model and was determined to be $2.8 R_S$ (as opposed to $D = 3.0 R_S$ originally used in the Connerney et al. model). With the assumption that the ring current density is proportional to $\frac{1}{\rho}$, (where $\rho = \sqrt{x_S^2 + y_S^2}$) the magnitude of the current system that best fit the V1 and V2 data is

$$J = \frac{I_0}{\rho} \quad \text{for } a \leq \rho \leq b \text{ and } |z| \leq D, \quad (3)$$

where $I_0 = 2.9 \times 10^6 \frac{A}{R_s}$ (which is $\frac{3}{4}$ the value of I_0 initially determined in the Connerney et. al. model). The magnetic field generated by the current system is then calculated using the Biot - Savart Law,

$$\vec{B}_{RC} = \frac{\mu_0}{4\pi} \int \frac{(\vec{Id\ell} \times \hat{r})}{r^2}, \quad (4)$$

where $\vec{r} = \vec{r} - \vec{r}'$ is the displacement from the current source at r' to the point of observation r as seen in Figure 2.

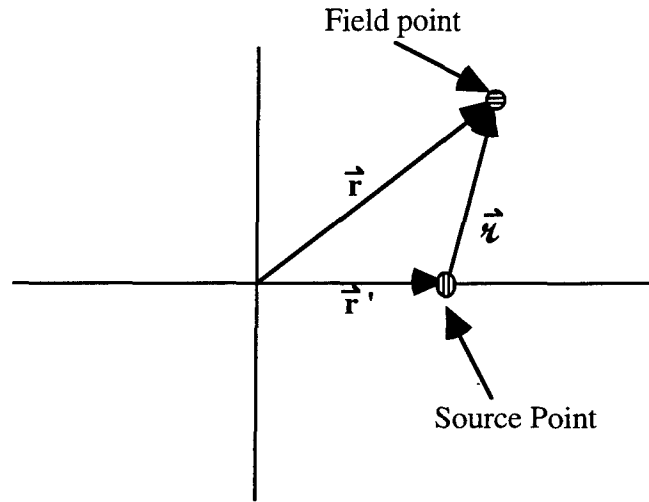


Figure 2. Graph showing the relationship between the vectors, \vec{r} , \vec{r}' and \vec{r} . The graph does not have axes labeled because it is in generalized coordinates.

The plasma ring current moves in the $\hat{\phi}$ direction and produces a magnetic field "upward" (in the same direction as the dipole moment of Saturn) inside the ring and "downward" outside the ring. Consequently, the superposition of the ring current magnetic field with the dipole field should cause reinforcements of magnetic field inside the ring current ($x_s < 8 R_s$) and cancellations outside the ring current ($x_s > 15.5 R_s$). Consequently, the addition of an extended ring current causes a departure from the pure

magnetic dipole presented in equation (1). The effect of adding a ring current magnetic field to the dipole magnetic field is that field lines are "stretched out" for higher latitude starting points in accordance with the observations made by V1 and V2 mentioned above. This stretching effect can be seen in Figure 2.

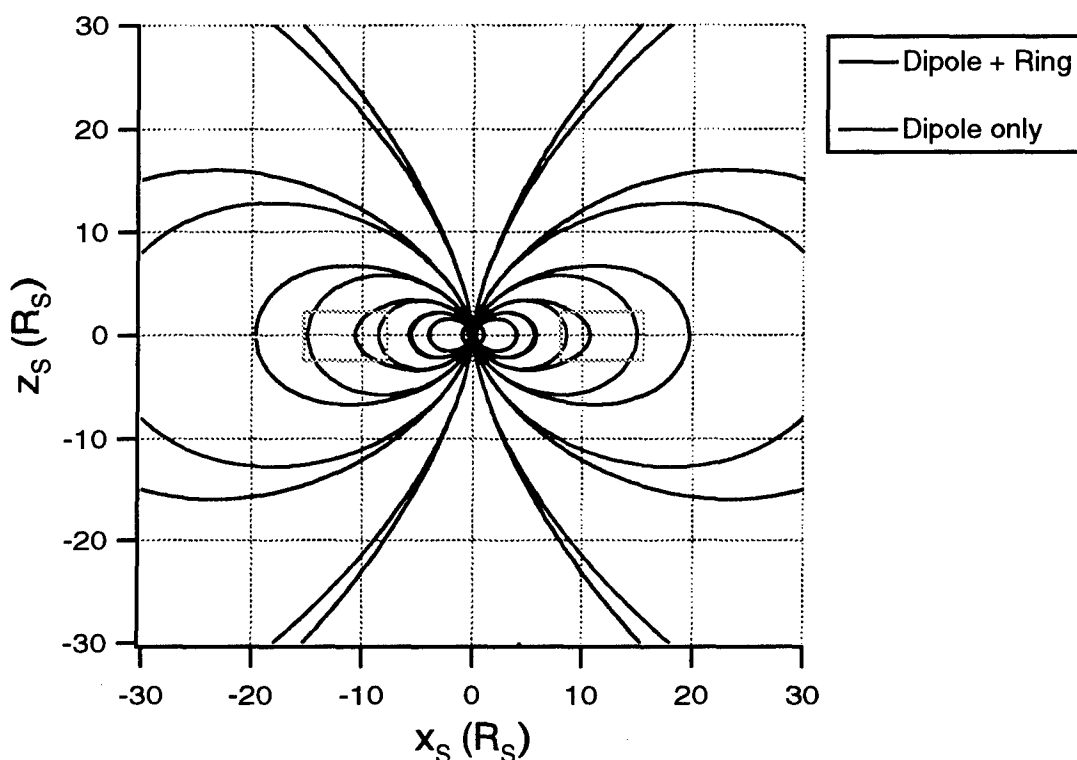


Figure 3. A graph of both the magnetic field due to the dipole and ring current contributions in the noon-midnight plane, as well as an overlay plot of the dipole field alone for comparison. The rectangular regions in the Figure indicate the edges of the cross section of the ring current model.

The lower density of the blue field lines relative to the red field lines seen around the magnetic equator at $x_s > 16 R_s$ clearly shows the cancellation effects of the ring current magnetic field with the dipole magnetic field resulting in a lower net magnetic field.

C. Determination of the shape of the magnetopause magnetic field

Methods involving the formation of the shape of the Earth's magnetopause boundary resulting from the interaction of the solar wind with the magnetosphere have been developed for during the past forty years. The original models were developed by Beard in 1960 and Mead and Beard in 1964 and then applied to the outer planets by Engle and Beard in 1980. Looking at the region near the subsolar point is useful in understanding the physics underlying the formation of the magnetopause. (The subsolar point is the point nearest to the sun on the magnetopause surface in the planetary magnetic field coordinate system. The subsolar point distance measured from the center of Saturn to the subsolar point will be designated as R_{Sub}).

First, assume that the region near the subsolar point can be approximated as a plane with a constant magnetic field directed inward toward the page.

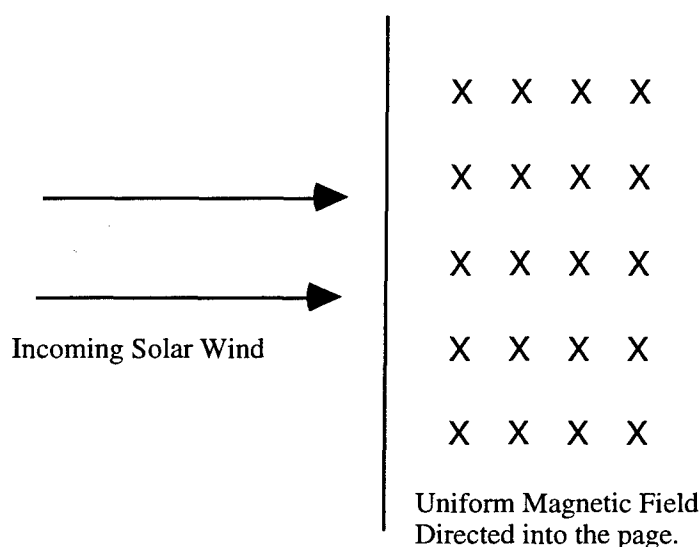


Figure 4. Diagram that shows the simplified version of Solar Wind incident upon the subsolar point of Saturn. The orientation of the Figure assumes a view looking down on the magnetic equator of the planet.

Considering how spatially large this region actually is, this is not a very extreme assumption. The solar wind incident from the left upon this plane is composed of equal

numbers of positive ions and negative electrons. Upon crossing the hypothetical magnetic boundary, each ion and electron will be subject to the Lorentz force.

$$\vec{F}_{\text{Lorentz}} = q_{\text{ion}}(\vec{v}_{\text{ion}} \times \vec{B}) \quad (5)$$

The consequence of this interaction is that positive ions will be deflected upward and the electrons will be deflected downwards. A simplified representation of this effect, composed of one positive ion (usually a proton) and its associated electron counterpart, is shown in Figure 5.

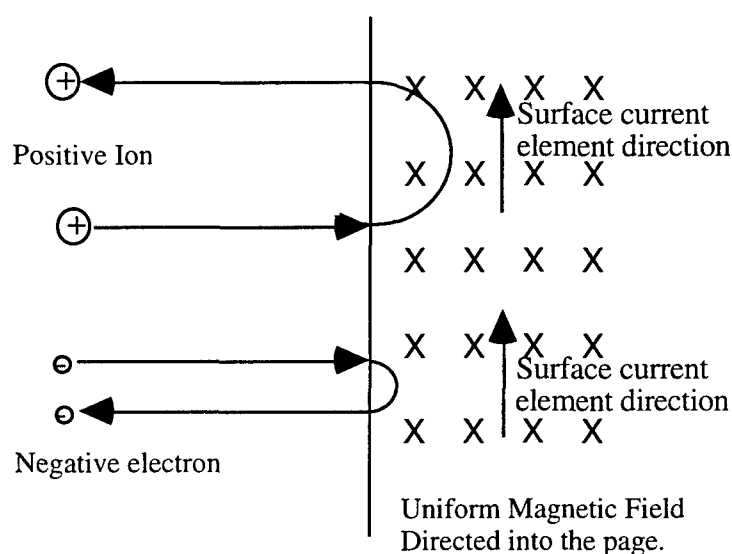


Figure 5. Diagram that shows the interaction of any plasma constituent incident upon a uniform magnetic field. Since an electron has the opposite charge of the positive ion, their associated current element will be in the upward direction. Consequently, the interaction of both particles with the magnetic field produce a current element in the upward direction.

This deflection generates a localized current system, with contributions from both the electrons and ions, each directed upward just inside the surface of the plane. The general trends of the individual current elements on the magnetopause surface will still follow the deflection characteristics shown in Figure 5 even if the solar wind is composed of a statistical sample of positive ions and negative electrons and the curvature of the magnetosphere is considered. The mathematics, however, require a more general approach than just the Lorentz force law. The resultant equation, which

accounts for magnetopause curvature and solar wind plasma, is given in equation (32) and will be discussed in depth later in this paper. By applying the Biot - Savart law to the magnetopause surface current elements, the magnetopause magnetic field can be obtained.

$$\vec{B}_{SC} = \frac{\mu_0}{4\pi} \int \frac{(\vec{Id}\vec{\ell}' \times \hat{r})}{r^2} \quad (6)$$

If one makes a fist with the right hand and then points the thumb in the direction of the surface current elements in Figure 5, the right hand rule of magnetic fields states that the direction of the magnetic field will loop around the current elements in the same direction that their fingers are pointing. Thus, the magnetic field generated by the magnetopause surface currents provides a reinforcement to the existing magnetic field on the inner side of the current system and a cancellation on the outer edge of the magnetosphere. This is essentially how the magnetopause surface is formed. Under stable conditions, the particles incident upon the magnetosphere generate a current system such that the resulting magnetic field doubles the magnitude of the non-localized, magnetosphere magnetic field just inside the magnetopause and provides a complex cancellation just outside the magnetopause. The system addressed above provides an ample physical model of how the magnetic field of the magnetopause is formed. The approach, however, is dependent upon the shape of the magnetopause.

The determination of the shape of the magnetopause is accomplished by attaining a pressure balance between the magnetic energy density pressure and the Newtonian solar wind pressure.

1. Newtonian solar wind pressure

The Newtonian dynamic solar wind pressure is determined directly from the momentum flux density. Given a fluid comprised of particles, s , with a particle number density n_s , velocity of magnitude v_s , and mass m_s , the pressure associated with the momentum flux density is

$$P_{flux} = n_s m_s (v_s)^2 \quad (7)$$

If the solar wind is incident upon a curved surface like the magnetopause, then only the portion of the solar wind pressure that is normal to the surface contributes to the magnetopause currents. Consequently,

$$P_{\text{flux}\perp} = n_s m_s (v_s \cos \chi)^2 \quad (8)$$

where χ is the angular orientation of the solar wind with respect to the normal to the magnetopause surface. Another way to represent this spatial variation is

$$P_{\text{flux}\perp} = P_{\text{solar wind}\perp} = n_s m_s (v_s)^2 |\hat{n}_s \cdot \hat{v}_s|^2 \quad (9)$$

where \hat{n}_s is a unit vector normal to the surface of the magnetopause.

The unit vector, \hat{n}_s , must be represented as a function in spherical coordinates in order to convert equation (9) to an appropriate form for calculation purposes. This can be accomplished by "surface-mapping" the magnetopause. Given that r can be described in terms of a position function, $r = R(\theta, \phi)$, a function $F(r, \theta, \phi)$ can then be defined as

$$F(r, \theta, \phi) = r - R(\theta, \phi) = 0 \quad (10)$$

The gradient of $F(r, \theta, \phi)$ is normal to $F(r, \theta, \phi)$ and consequently normal to the surface of the magnetopause. Explicitly, the gradient of $F(r, \theta, \phi)$ is equal to

$$\vec{\nabla} F(r, \theta, \phi) = \vec{\nabla} r - \vec{\nabla} R(\theta, \phi) = \left[\frac{\partial r}{\partial r} \hat{r} \right] - \left[\frac{1}{r} \frac{\partial R}{\partial \theta} \hat{\theta} + \frac{1}{r(\sin \theta)} \frac{\partial R}{\partial \phi} \hat{\phi} \right] \quad (11)$$

To find the unit vector normal to the surface, divide the gradient of $F(r, \theta, \phi)$ by its magnitude.

$$\hat{n}_s = \frac{\vec{\nabla} F(r, \theta, \phi)}{|\vec{\nabla} F(r, \theta, \phi)|} = \frac{1}{K} \left[\hat{r} - \frac{1}{r} \frac{\partial R}{\partial \theta} \hat{\theta} - \frac{1}{r(\sin \theta)} \frac{\partial R}{\partial \phi} \hat{\phi} \right] \quad (12)$$

$$\text{where } K = \sqrt{\left[1 + \left(\frac{1}{r} \frac{\partial R}{\partial \theta} \right)^2 + \left(\frac{1}{r(\sin \theta)} \frac{\partial R}{\partial \phi} \right)^2 \right]}$$

2. Magnetic pressure

The equation for magnetic pressure is derived from the momentum equation of magnetohydrodynamics. To see the extensive mathematical approach from this initial assumption, see Appendix B [Kivelson *et al.*, 1995]. The magnitude of the magnetic pressure is concluded to be

$$P_B = \frac{B^2}{2\mu_0} \quad (13)$$

Equation (13) must be re-written to account for the relationship between the magnetopause shape and magnetic field direction. By taking the cross product of the unit vector normal to the magnetopause surface with the net magnetic field vector, the following result is obtained:

$$P_B = \frac{|\hat{n}_s \times \vec{B}|^2}{2\mu_0} \quad (14)$$

3. Pressure balance

If a pressure balance is assumed between the magnetosphere and the incident solar wind, then equation (9) is equal to equation (14).

$$\frac{|\hat{n}_s \times \vec{B}|^2}{2\mu_0} = (n_s m_s (v_s)^2) |\hat{n}_s \cdot \hat{v}_s|^2 \quad (15)$$

Equation (15) can be simplified to

$$|\hat{n}_s \cdot \hat{v}_s|^2 = \eta |\hat{n}_s \times \vec{B}|^2 \quad (16)$$

where $\eta = (2\mu_0 n_s m_s (v_s)^2)$.

If the subsolar point is chosen as a reference point where the normalized magnetic field is set equal to 1, then equation (16) can be further simplified such that η is normalized to 1. By taking the square root of both sides of this simplified form of equation (16), the resulting equation is

$$|\hat{n}_s \cdot \hat{v}_s| = |\hat{n}_s \times \vec{B}_n| \quad (17)$$

In equation (17), \vec{B}_n is normalized everywhere on the surface relative to $|\vec{B}| = 1$ at the subsolar point. Equation (17) is then used to determine the shape of the magnetopause magnetic field.

To calculate the magnetopause shape, the region around the planet is broken into a 5° by 5° grid in θ and ϕ . For a particular point on the grid (corresponding to a particular value of θ and ϕ), the value of r is varied over a predetermined range. If the range is selected appropriately, then a value of r should be obtained which satisfies equation (17). This value of r is where the magnetopause surface is located for that particular grid point. By doing these calculations over the entire range of θ and ϕ , ($0^\circ < \theta < 180^\circ$, $0^\circ < \phi < 360^\circ$), the magnetopause shape is determined.

D. Magnetotail contribution

For Earth, spacecraft observations have confirmed that a cross-tail current sheet with its associated return currents generates a magnetotail magnetic field which provides an additional contribution to the planetary magnetospheric field [Behannon, 1968]. The current sheet is formed by the rejoining of deflected solar wind particles after they have traveled past the planet following deflection from their original paths by interaction with the magnetospheric field. These particles generate a dawn-to-duskward cross-current as they re-merge to eventually form a neutral plasma streaming outwards. These observations lead us to predict that a magnetotail magnetic field is generated by the existence of a neutral current sheet on the night side of Saturn as well. The orientation of the cross-current sheet for Saturn is shown in Figure 6.

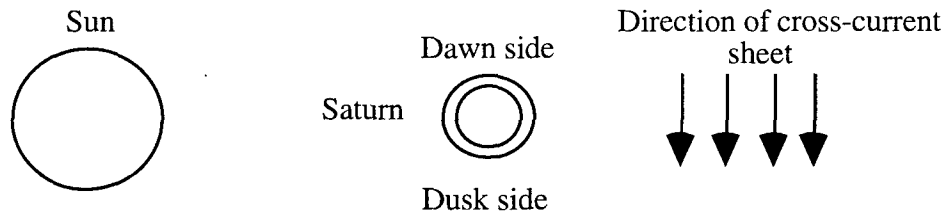


Figure 6. An overhead view looking down on the northern hemisphere of Saturn in order to show the direction of the cross-current sheet in the night side of the planet.

Unfortunately, both V1 and V2 exited the magnetopause at $x_s \approx -30 R_s$ and thus acquired very little data to use for an accurate Saturn magnetotail model [Ness *et al.*, 1981].

To provide a first order extension to the Saturnian model via the incorporation of a magnetotail, an analogy of the 1979 Beard magnetotail model is assumed. The Beard model is a hybrid in that the vector potential, \vec{A} , (where $\vec{B} = \vec{\nabla} \times \vec{A}$) is determined from magnetohydrodynamics and then the parameters are empirically fit to Earth satellite data. It assumes a variation of the 1962 Harris sheet model of a current sheet with a finite thickness, z_0 [Harris, 1962]. The Harris sheet model was obtained by solving the Vlasov equation, which is a magnetohydrodynamic equation relevant to the plasma system. The resulting magnitude of the vector potential obtained after obtaining the solutions to the Vlasov equation and applying the necessary boundary conditions and assumptions is

$$A = \alpha + \beta \left[\ln \cosh\left(\frac{z}{z_0}\right) \right]. \quad (18)$$

where α and β are arbitrary constants to be ultimately fit to satellite observations. As stated above, z_0 represents the neutral current sheet thickness. For Earth, this was approximated to be $4 R_e$. For a given x , the A_y and A_z components of a general vector potential can be expressed as a series expansion.

$$A_y = A_0 + A_1|z| + A_2|z|y^2 + A_3z^2 + A_4y^2; \quad z \neq 0 \quad (19)$$

$$A_z = \sum_{j=1}^3 \sum_{i=1}^{4-j} (A_{ij}y^{2i-1} z^{2j-1}) \quad (20)$$

The Harris finite sheet vector potential was then incorporated into the general expansion, equation (19), to obtain

$$A_y = f(x) \left\{ (A_0 + A_1z_0 \ln(2)) + A_1z_0 \left[\ln \cosh\left(\frac{z}{z_0}\right) \left(1 + \frac{A_2}{A_1}y^2\right) \right] + A_3z^2 + A_4y^2 \right\} \quad (21)$$

The x - dependence of the tail is determined from $f(x)$. The function $f(x)$ is based on the product of two terms. The first term, $g(x)$, represents the x dependence of the current of the magnetotail system.

$$g(x) = \frac{K_x}{(b-x)^n} \quad (22)$$

where K_x is a constant of proportionality and b is the subsolar distance of the planet. Since there are no satellite data in the tail for Saturn, the value of K_x was determined in accordance with observations made in the Earth magnetosphere system. For $B_x = 11$ nT at $x_e = -60 R_e$, $y_e = 0.0 R_e$, $z_e = 12 R_e$, K_x is equal to 4.891. The second term, $h(x)$, represents the physical characteristics of the tail at its near Earth position starting point.

$$h(x) = 1 - \exp[-\alpha(b-x)^s]. \quad (23)$$

The constant α is chosen to give a minimum value of B_z at $x = -b$. The exponent parameter, s , is used to determine how much the magnetotail is attenuated in the x direction.

$$\alpha = \frac{(s-1)}{s(2b)^s} \quad (24)$$

For the Earth magnetosphere, with $b = 10 R_e$ and $s = 4.0$, then $\alpha = 4.69 \times 10^{-6}$.

By taking the product of $g(x)$ and $h(x)$, the resulting function, $f(x)$, is found to be

$$f(x) = g(x)h(x) = \frac{K_x}{(b-x)^n} (1 - \exp[-\alpha(b-x)^s]). \quad (25)$$

The coefficients of A_y and A_z were then fit to Earth magnetometer satellite data by the method of least squares to obtain

$$\begin{aligned} A_y = f(x) & (100.7 + 5.57z_0 - 8.04z_0[\ln \cosh(\frac{z}{z_0})(1 - \Phi y^2)] \\ & + 0.150z^2 - 0.107y^2) \end{aligned} \quad (26)$$

$$\begin{aligned} A_z = f(x) & [0.321yz - (1.555 \times 10^{-4})yz^3 + (2.471 \times 10^{-7})yz^5 \\ & + (2.865 \times 10^{-4})y^3z - (1.036 \times 10^{-6})y^3z^3 - (1.173 \times 10^{-7})y^5z] \end{aligned}$$

The value of Φ is determined by approximating where the boundary of the magnetotail terminates in the x-y plane. For the Earth system, assuming that, under steady state conditions, the near-tail terminates at approximately $20 R_e$, Φ was calculated to be 0.00052. It should be noted that the fitted coefficients for this model are based on satellite magnetometer data found in the Earth magnetotail. Also, an important feature of the model is that the coefficients were determined such that the magnetic field value of B_z terminates at the Earth magnetotail boundary in the y-z plane at $z_e = 10 R_e$. By taking the curl of the vector potential components shown in equation (26), the resulting magnetic field components are

$$\begin{aligned}
B_x = f(x) \{ & 0.021z - (1.555 \times 10^{-4})z^3 + (2.471 \times 10^{-7})z^5 \\
& + (8.595 \times 10^{-4})y^2z - (3.108 \times 10^{-6})y^2z^3 - (5.865 \times 10^{-7})y^4z \\
& + 8.04[\tanh(\frac{z}{z_0})(1 - \Phi y^2)](1 - \Phi y^2) \}
\end{aligned} \tag{27}$$

$$\begin{aligned}
B_y = -f'(x) \{ & 0.321yz - (1.555 \times 10^{-4})yz^3 + (2.471 \times 10^{-7})yz^5 \\
& + (2.865 \times 10^{-4})y^3z - (1.036 \times 10^{-6})y^3z^3 - (1.173 \times 10^{-7})y^5z \}
\end{aligned}$$

$$\begin{aligned}
B_z = f'(x) \{ & 100.7 - 5.57z_0 - 8.04z_0[\ln \cosh(\frac{z}{z_0})(1 - \Phi y^2)] \\
& + 0.150z^2 - 0.107y^2 \}
\end{aligned}$$

One of the great advantages of the Beard model is that its analytical form can be easily shown to obey the conservation of magnetic flux, i.e. $\vec{\nabla} \cdot \vec{B} = 0$. The divergence of the magnetic field components in equations (27) are everywhere zero, thus ensuring flux conservation throughout the neighborhood of the magnetotail.

In order to ensure appropriate adaptation to the Saturnian system, it is essential that the boundary conditions of the Beard magnetotail model are obeyed in the Saturnian magnetosphere. First, B_z must terminate at an approximated Saturn magnetotail boundary in the y-z plane. The location of the Saturnian magnetotail was determined by taking the ratio of the subsolar point distances of the two planets.

$$z_{\text{Saturn termination}} = \left(\frac{R_{\text{Subsolar Saturn}}}{R_{\text{Subsolar Earth}}} \right) (z_{\text{Earth termination}}) = 48 R_s \tag{28}$$

In order to make this adaptation, the spatial values in the z direction must be transformed such that a z value of $48 R_s$ in the Saturn coordinate system corresponds to a z of $20 R_e$ in the Earth system. By reducing the z coordinate in the Beard model by a factor of $\frac{1}{2.4}$, this is accomplished.

$$z_{\text{Saturn}} = \frac{R_{\text{Subsolar Earth}}}{R_{\text{Subsolar Saturn}}} (z_{\text{Earth}}) = \frac{z_{\text{Earth}}}{2.40} \tag{29}$$

In each case, the coordinate system for the planet being analyzed is in units of its respective planetary radii. In other words, z_{Earth} and $R_{\text{Subsolar Earth}}$ are represented in

units of Earth radii and z_{Saturn} and $R_{\text{Subsolar Saturn}}$ are represented in units of Saturnian radii.

From observation of the ME95 magnetopause, it is predicted that some flaring should occur. Flaring is a departure from the cylindrical shape of the magnetotail magnetic field as the distance of the magnetopause increases for an increasing x_s on the night side of Saturn. One inconsistency in the transformation shown in equation (29) is that it does not account for the flaring of the magnetotail on the night side. Thus, any B_z magnetic field component that exists outside the tail boundary due to flaring of the tail in the global magnetosphere model will be assumed to be zero. This assumption, however, does not cause considerable differences to the overall physical characteristics of the model, considering the small value of B_z near the magnetopause boundary.

A similar transformation is also necessary in the y direction. The transformation of the y direction is different than that obtained in the z direction due to the inclusion of a ring current in the Saturnian magnetosphere. Thus, the Saturnian magnetosphere is more elliptical than the spherically shaped Earth magnetosphere as viewed in the dawn-dusk meridian. A good measure of the "deviation from sphericity" of the Saturnian magnetosphere in the dawn-dusk meridian is the ratio between the "flatness" and "bluntness" of the magnetopause as defined in the ME95 paper. Flatness is the ratio of the pole point height (pole point height is the position of the magnetopause on the positive z axis) of the planet to the subsolar distance. Bluntness is the ratio of the distance from the magnetopause to the planet in the dawn-dusk meridian to the subsolar distance. By taking the ratio of the flatness and bluntness of the ME95 model, the "deviation from sphericity" factor, Γ_{dev} , is obtained. For the ME95 model, $\Gamma_{\text{dev}} = 1.262$. Thus, rather than merely divide the y coordinates of the Saturnian magnetotail by 2.4 in accordance with the subsolar ratio distances between Saturn and Earth as in equation (29), an additional factor, $\frac{1}{1.262}$, is necessary to account for the elliptical properties of the magnetotail model.

$$y_{\text{Saturn}} = \frac{R_{\text{Subsolar Earth}}}{(R_{\text{Subsolar Saturn}})(\Gamma_{\text{dev}})}(y_{\text{Earth}}) = \frac{y_{\text{Earth}}}{3.029} \quad (30)$$

Another necessary modification to develop the Saturn analogy of the Beard magnetotail model is that the location of the starting point of the tail must be adjusted. As discussed above, the inclusion of the ring current causes magnetic field lines to be "stretched out" for a given co-latitude starting point on the planet surface. Since Earth

does not have a significant magnetic field perturbation from its ring current system, the Beard magnetotail model selects a distance of one Earth-subsolar point away from the planet on the night side as the starting point of the tail. In order to adapt the Saturn model, however, the starting point of the tail will be more distant in the night region due to the field lines being stretched out from the effects of the ring current. By using a field-trace program which only contains the effects of the dipole plus solar wind magnetic contributions, a co-latitude angle could be determined which was associated with a crossing of the magnetic equatorial plane at $x_s = -24 R_s$. This co-latitude angle was then used as a starting point for a new field trace which contains the dipole, ring current and solar wind magnetic field contributions. The starting point of the magnetotail is at the same location where the new field line crosses the magnetic equator in the noon-midnight meridian. For the ME95 model, the starting point of the magnetotail occurs at $x_s = -28.60 R_s$. Thus, the constant b in equations (24 and 25) must be multiplied by 1.19 to obtain the correct attenuation in the x direction for the Saturnian magnetosphere model, giving a new α equal to 7.01×10^{-8} . The resulting trends of the Saturn magnetotail can be seen in Figures 7-9 and are shown in good agreement with Figures 4-6 of the Beard magnetotail model. It should be noted that the dipole moment of Saturn is aligned parallel to the spin axis direction, whereas Earth's dipole moment is aligned anti-parallel with respect its spin axis. Consequently, the ordinate in the graphs below are represented as negative magnetic field values to provide a direct comparison with the 1979 Beard results.

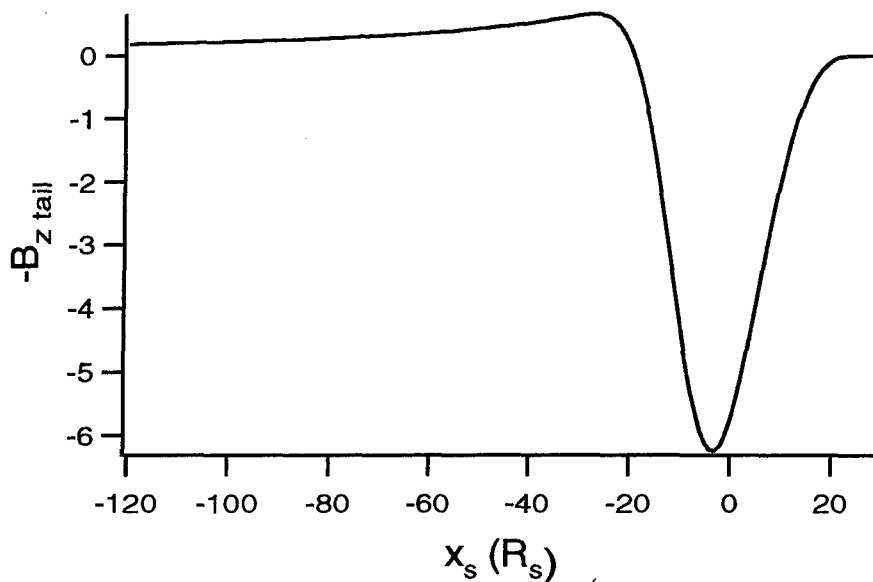


Figure 7. Plot of $-B_{z\text{tail}}$ as a function of x in units of Saturnian radii. The units of $B_{z\text{tail}}$ are in arbitrary units normalized to the K_{tail} coefficient discussed below. The x -coordinate is defined such that it is pointing towards the Sun in the positive direction.

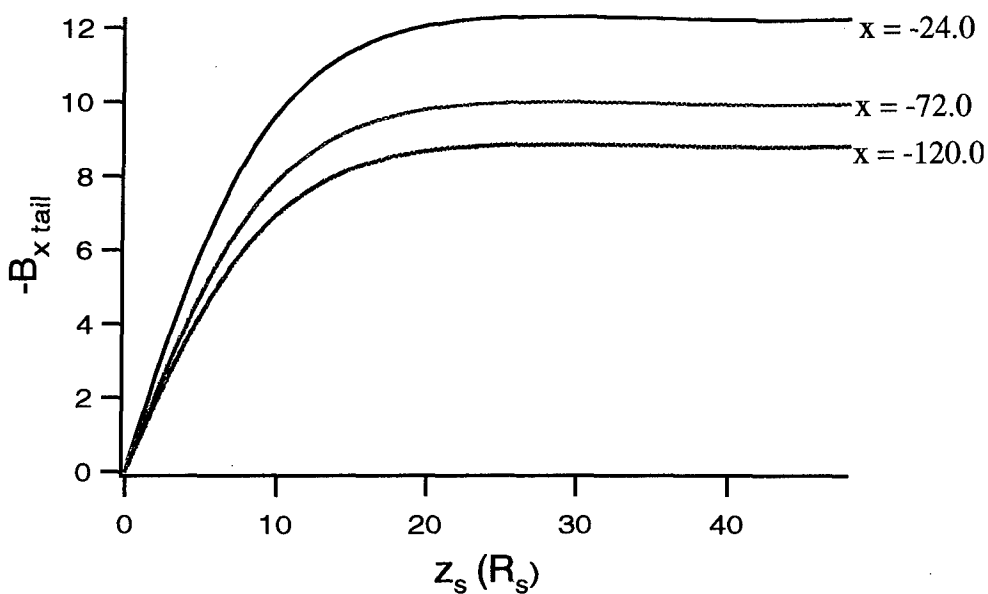


Figure 8. Plot of $-B_{z\text{tail}}$ as a function of z for $x = -24, -72$ and -120 as shown in the graph. The units of $B_{z\text{tail}}$ are in arbitrary units normalized to the K_{tail} coefficient discussed below. All distances are in units of Saturnian radii. The z -coordinate is defined such that it is aligned with the dipole axis of Saturn.

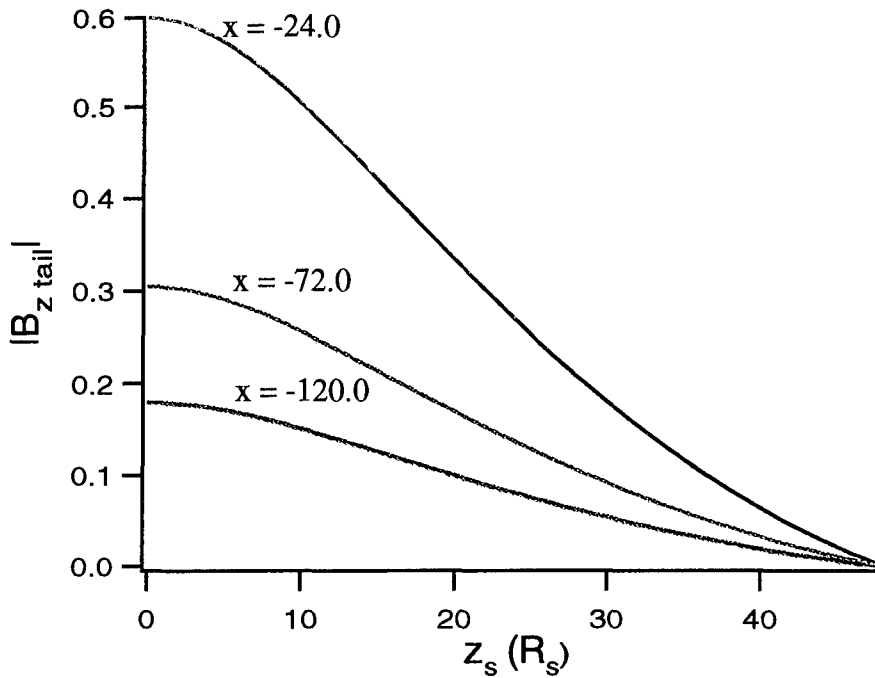


Figure 9. Plot of $-B_{z \text{ tail}}$ as a function of z for $x = -24, -72$ and -120 as shown in the graph. The units of $B_{z \text{ tail}}$ are normalized to the K_{tail} coefficient discussed below. Note how the magnetic field terminates at $z = 48 R_s$.

The magnitude of the Beard magnetotail system is adjusted to coincide with magnetic field values found around Saturn by multiplying the magnetic field components of the tail by an attenuation coefficient, K_{tail} , prior to superposition with the other magnetospheric contributions. K_{tail} is defined as the ratio of the magnitude of the steady state magnetic field values determined at the subsolar point of the planets. For Earth, the steady state value of the magnetic field at the subsolar point is approximated to be 66.1448 nT and Saturn's magnetic field value is approximated to be 2.438 nT as taken from the ME95 model. Thus, K_{tail} is evaluated to be approximately 0.037.

One important final point about the adapted version of the Beard magnetotail model to Saturn is that no adjustments were made to the coefficients of equation (27). Instead, a spatial transformation was applied to the Saturnian magnetotail system to ensure continuation with the functional behaviors shown in Figures 4-6 of the Beard model. This transformation can be quantitatively represented as

$$\begin{bmatrix} x_{\text{Saturn}} \\ y_{\text{Saturn}} \\ z_{\text{Saturn}} \end{bmatrix} = \begin{bmatrix} 1 & 0 & 0 \\ 0 & \frac{1}{3.029} & 0 \\ 0 & 0 & \frac{1}{2.4} \end{bmatrix} \begin{bmatrix} x_{\text{Earth}} \\ y_{\text{Earth}} \\ z_{\text{Earth}} \end{bmatrix} \quad (31).$$

This transformation can be envisioned as compressing the Saturnian spatial elliptical magnetotail locations into the fixed region defined by the Earth magnetotail dimensions. It is necessary to adapt the model in this fashion to maintain the claim that the divergence of the magnetotail magnetic field components remains zero in accordance with flux conservation. If the coefficients were directly changed, this would no longer necessarily be true. Graphs of the magnetic field due to just the magnetotail contribution for Saturn are shown in Figure 10 and 11.

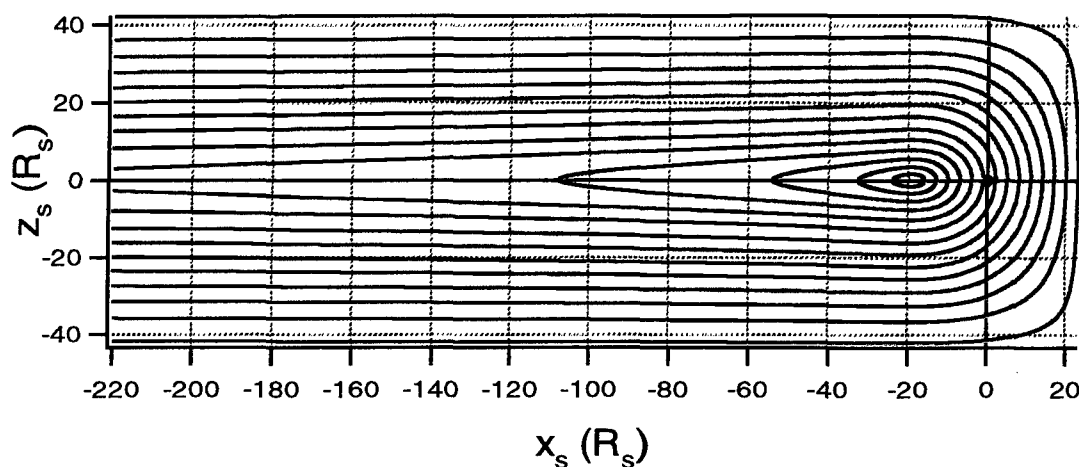


Figure 10. Noon-midnight meridian field tracing of the magnetotail magnetic field for Saturn. The coordinate system is centered on the planet with the positive x coordinate pointing towards the sun and the z axis aligned with the magnetic dipole axis of Saturn.

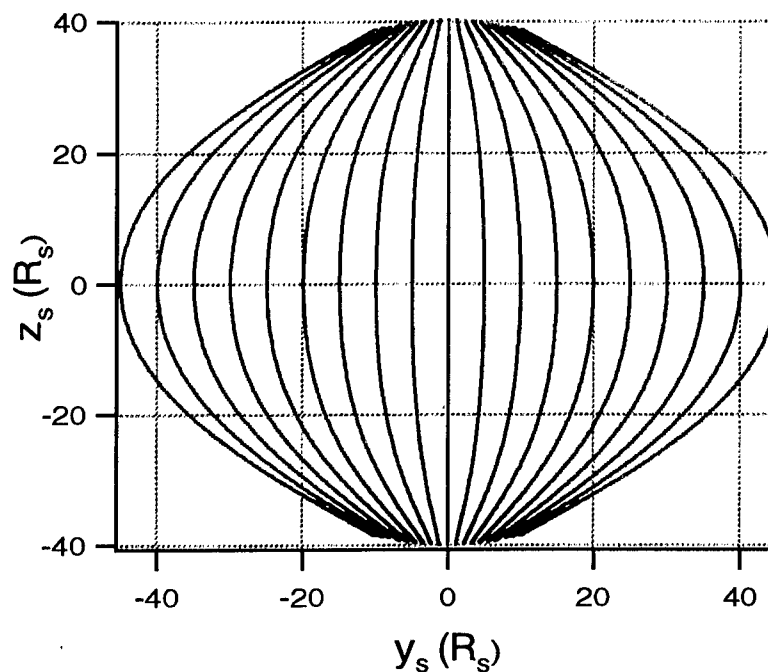


Figure 11. Projection of the magnetotail magnetic field for Saturn in the y - z plane. The coordinate system is centered on the planet with the x - y plane parallel to the magnetic equator and the z axis aligned with the magnetic dipole axis of Saturn. Notice the ellipsoidal characteristics of the Saturnian magnetotail due to the transformation via equation (31).

III. Method of generating a self-consistent model using the above contributions

The first step in creating the magnetosphere model for Saturn is to calculate the current elements on the magnetospheric surface based on the magnetopause shape as determined by the pressure balance in equation (16). After the zeroth order surface is generated (zero is used as the first order since some of the contributions to the magnetopause magnetic field are not even valid at this point), a corresponding set of magnetopause current elements can be produced. These current elements are calculated by taking the cross product of the unit vector normal to the magnetopause surface and the net magnetic field on the magnetopause surface.

$$\vec{J} = -\hat{n}_s \times \vec{B}_{\text{net}} \quad (32)$$

The net magnetic field is comprised of the four magnetic field contributions discussed above, $\vec{B}_{\text{net}} = \vec{B}_D + \vec{B}_{RC} + \vec{B}_{SC} + \vec{B}_{\text{tail}}$. In spherical coordinates, the resulting cross product of equation (32) in its expanded form is

$$\begin{aligned}\vec{J}_R &= \left[\frac{B_{\theta \text{ net}}}{R(\sin(\theta))} \frac{\partial R}{\partial \phi} - \frac{B_{\phi \text{ net}}}{R} \frac{\partial R}{\partial \theta} \right] \hat{r} \\ \vec{J}_\theta &= -\left[\frac{B_{r \text{ net}}}{R(\sin(\theta))} \frac{\partial R}{\partial \phi} + B_{\phi \text{ net}} \right] \hat{\theta} \\ \vec{J}_\phi &= \left[B_{\theta \text{ net}} + \frac{B_{r \text{ net}}}{R} \frac{\partial R}{\partial \theta} \right] \hat{\phi}\end{aligned}\tag{33}$$

The current elements in equation (33) are then used to find the next order magnetic field contributions using the Biot - Savart Law, equation (6), as discussed above. These magnetic field values are calculated just on the magnetopause. With a new set of magnetic field values for the magnetopause, a new refined magnetopause shape is obtained. Consequently, a new set of net magnetic field values are generated on the magnetopause surface. This next order net magnetic field is then applied to equation (32) to obtain a new set of surface current elements. This procedure is repeated until the magnetic field values obtained from equation (6) converge. Mathematically, this is represented as

$$\vec{B}_{SC(n)} = \vec{B}_{SC(n-1)}\tag{34}$$

where $\vec{B}_{SC(n)}$ represents the last calculated set of magnetopause magnetic field values and $\vec{B}_{SC(n-1)}$ represents the previous iteration's set of magnetopause magnetic field values. This convergence also indicates a self-consistent magnetospheric model. Self-consistency implies that the shape of the magnetopause and the magnitude of the magnetic field values on the magnetopause are constant over consecutive iterations. This also implies that the magnetic field values inside the whole magnetosphere should be constant over consecutive iterations.

The resulting current elements from equation (33) of the last iteration are then used to determine the magnetic field values inside the global magnetosphere via the Biot - Savart law, equation (6), which will hereafter be labeled \vec{B}_{MP} . The integration is

applied everywhere inside the magnetosphere except on the surface. The contributions of the solar wind interaction on the surface for points inside the magnetosphere can be represented by the gradient of a scalar potential.

$$\vec{B}_{MP} = \vec{\nabla} \Phi_{MP} \quad (35)$$

The scalar potential can be represented as a series of spherical harmonics. Representing Φ in terms of spherical harmonics has, in the past, been successfully employed for modeling the magnetopause surface current contributions in a spherical neighborhood centered on the planet. This form is adopted here. Consequently, associated Legendre Polynomials were chosen as the basis to fit the theta-dependence of the series expansion. Periodic functions, $\cos(m\phi)$, are used for modeling the azimuthal dependence. The radial dependence factor of the expansion is represented as r^λ . Thus, the resulting magnetic scalar potential is represented as:

$$\Phi_{MP} = \sum_{\lambda=1}^{\lambda_{\max}} r^\lambda \sum_{m=0}^{\lambda} G_{\lambda,m} P_{\lambda}^m(\cos\theta) \cos(m\phi) \quad (36)$$

where $G_{\lambda,m}$ are coefficients used to fit the resulting magnetic field of the scalar potential expansion, $\vec{B}_{MP} = \vec{\nabla} \Phi_{MP}$, to the magnetic field components at locations well inside the magnetopause surface. Due to the r - dependence of the expansion, however, difficulties may arise regarding the fitting of the function at locations far from the origin and beyond the "sphere of applicability." The "sphere of applicability" is defined as the magnetospheric region around the planet where $r \leq R_{\text{sub}}$. For values of $r \geq R_{\text{sub}}$ on the nights side of Saturn, the r^λ factors cause a "blow up" of magnetic field values. Consequently, attenuating the magnetic field contributions, \vec{B}_{MP} , at regions beyond the "sphere of applicability" is necessary to maintain the features of the model. The resulting coefficients, $G_{\lambda,m}$, can then be used to generate the magnetospheric field contributions caused by the solar wind interaction when substituted back into equation (36).

IV. Observations of a self-consistent idealized global Saturnian model

The process of constructing a magnetosphere was executed through nine iterations, when reasonable self-consistency was obtained in the major features of the model. The resulting magnetic field contributions were then used to trace magnetic field lines to display the global magnetic field of the Saturnian magnetosphere. The corresponding expansion coefficients, $G_{\lambda,m}$, are given in Appendix C. A noon-midnight plot of the idealized Saturnian magnetosphere with its associated magnetopause is shown in Figure 12.

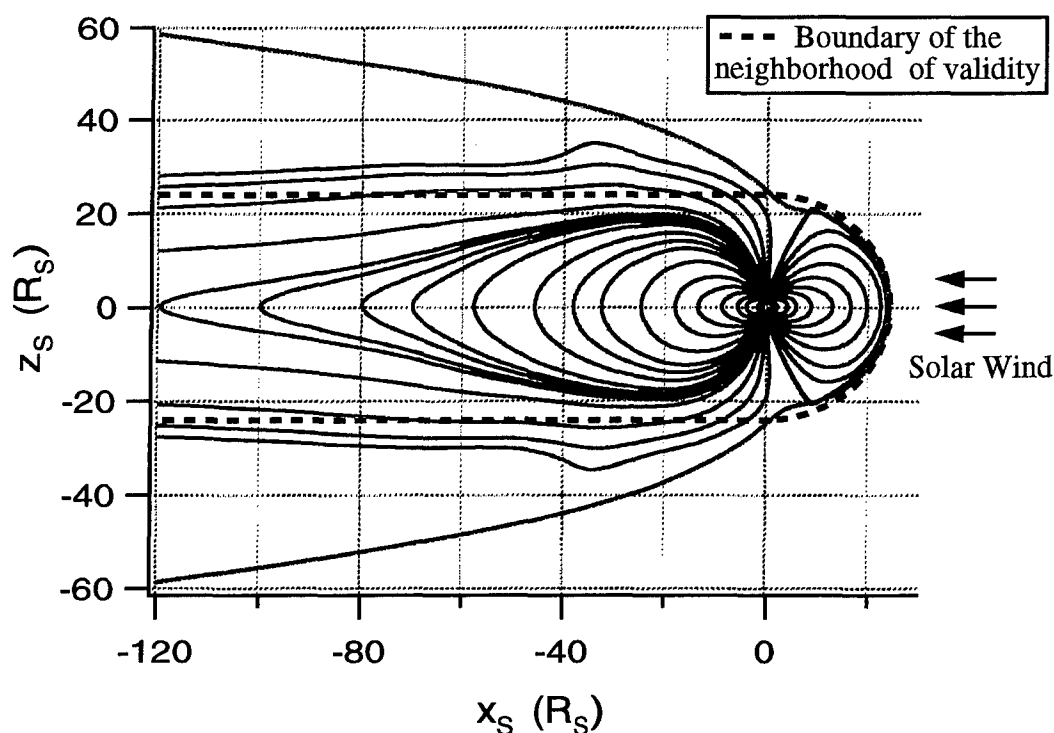


Figure 12. Trace of the idealized Saturnian magnetosphere and its associated magnetopause (in blue) in the noon-midnight meridian. The black dashed lines show approximately where the model is valid for observation.

The bumps that occur at $x_S = -38 R_S$ are un-physical artifacts which are predicted to go away after further iterations. The inclusion of the tail model has increased the range of validity of the Saturnian magnetosphere to the region shown by the dashed lines in Figure 12. In the ME95 model, the dashed lines were cut off at $x_S = -15 R_S$.

The separation of regions of magnetic field lines forming the frontal lobe and magnetic field lines streaming backwards occurred at an approximate co-latitude of 5° . This location is called the cusp. In the neighborhood of the cusp, the $|\hat{n}_S \cdot \hat{v}_S|$ term rapidly changes from a small to relatively large value for a meridian plot at a given longitude. It is also characterized by a change in the sign of the theta component of the net magnetic field just inside the magnetopause. The cusps lie on the day side of the magnetosphere and transition to smooth meridian lines with no inflection points before the dawn-dusk meridian.

Another feature of the model is the asymmetry of magnetic field lines between the day side and night side of the magnetosphere. Compression of field lines on both the day and night side is due to the incoming solar wind pressure. (The compression on the dayside, however, is more pronounced than on the night side). The extreme extension of field lines tailward in the night region is due to the magnetotail contribution to the model. The overall asymmetry characteristic of the model can be observed accurately by inspecting a series of field lines in 30° longitudinal increments for a co-latitude of 10° as in Figure 13.

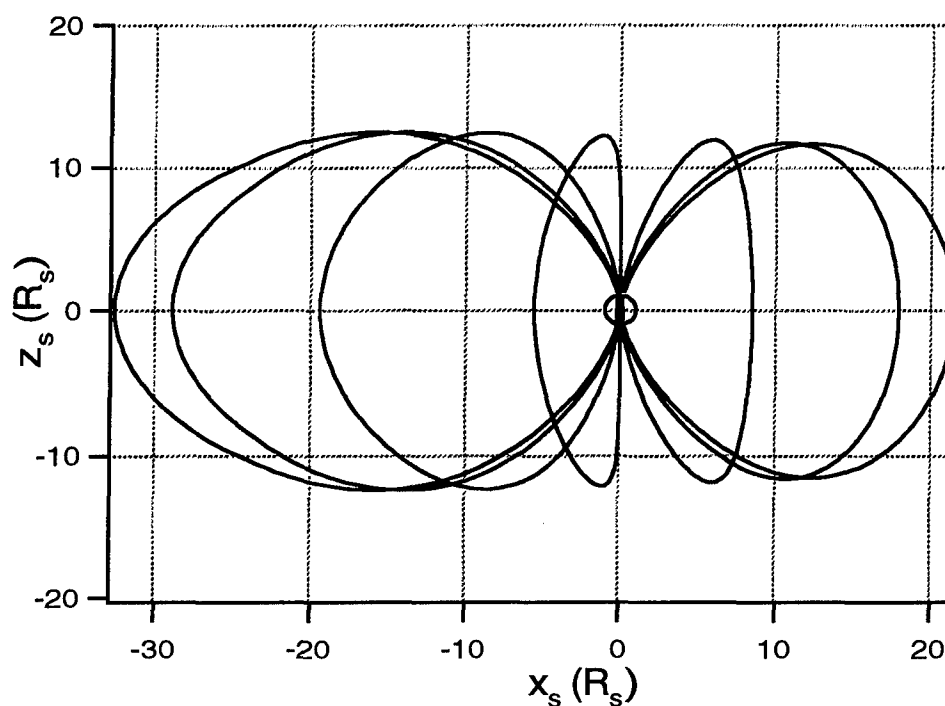


Figure 13. Projections of magnetic fields onto the noon-midnight meridian plane. These particular traces originate from the planet surface at a co-latitude of 10° and initial longitudes of 0° , 30° , 60° , 90° , 120° , 150° and 180° .

If a larger co-latitude is chosen, the effects attributable to the solar wind pressure and magnetotail contribution decrease due to the dominating effects of the interior contributions, \vec{B}_D and \vec{B}_{RC} . This can be seen by looking at a series of field lines in 30° longitudinal increments for a co-latitude of 30° as in Figure 14.

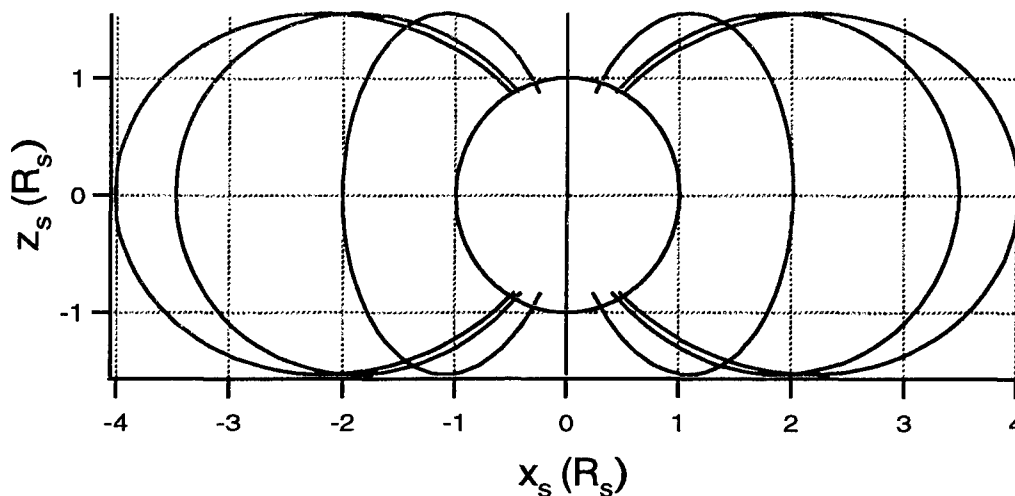


Figure 14. Projections of magnetic fields onto the noon-midnight meridian plane. These particular traces originate from the planet surface at a co-latitude of 30° and initial longitudes of 0° , 30° , 60° , 90° , 120° , 150° and 180° .

Notice the symmetry between the day and night side in Figure 14 as compared to Figure 13.

One final observation about the features of the idealized model is that the field lines at a given small co-latitude are non-axi-symmetric. In other words, a field line originating at a given small co-latitude and longitude will not have the same longitudinal value when observed at the magnetic equator. In addition, the magnetic field lines appear to "bend" due to the incoming solar wind pressure. These effects can be seen in Figure 15.

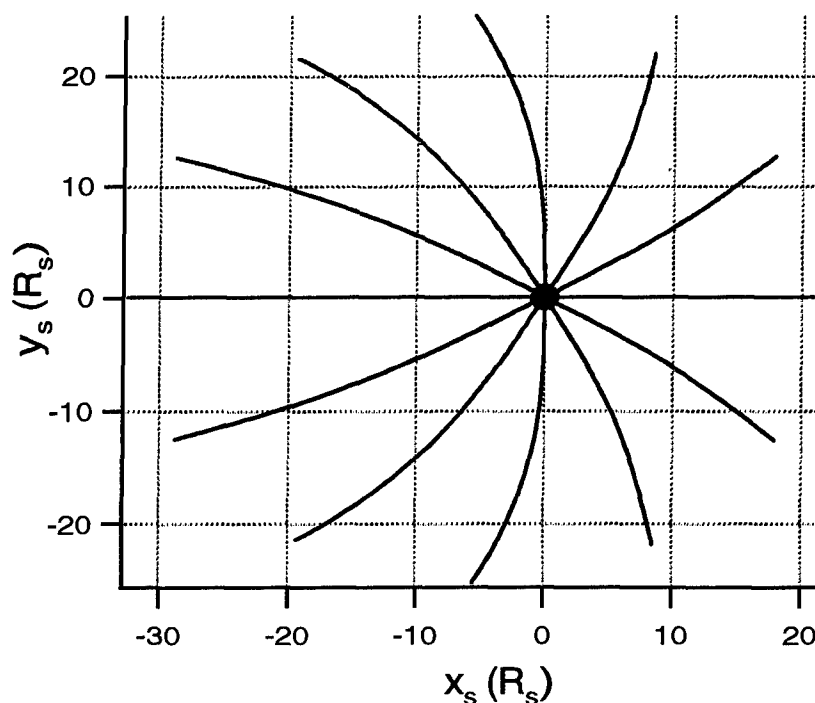


Figure 15. Projection of magnetic field lines onto the magnetic equatorial plane (x - y plane). These particular traces originate from the planet surface at a co-latitude of 10° and initial longitudes of 0° , 30° , 60° , 90° , 120° , 150° , 180° , 210° , 240° , 270° , 300° and 330° .

V. Validation of the Idealized Global Saturnian Model

The primary source of data for verification of the idealized Saturnian model is the V1 and V2 magnetometer data. Voyager 1 entered the Saturnian magnetosphere during quiescent conditions while Voyager 2 entered the magnetosphere during volatile solar wind conditions. It is suspected that Saturn passed inside the Jovian magnetotail during the V2 flyby leading to the relatively disturbed results [Lepping *et al.*, 1981]. Conveniently, both V1 and V2 both flew by Saturn during a period when the solar wind was nearly parallel to the magnetic equator, so the idealized model is the best representation of the Saturnian magnetosphere during the V1/V2 flybys.

As can be seen from the limited trajectory projections in Figure 16, Voyager 1 and Voyager 2 spent little time in the night region of Saturn. In the complete trajectories, Voyager 1 extended into the night region the farthest; exiting the magnetosphere at $x_s \approx -30 R_S$ [Ness *et al.*, 1981].

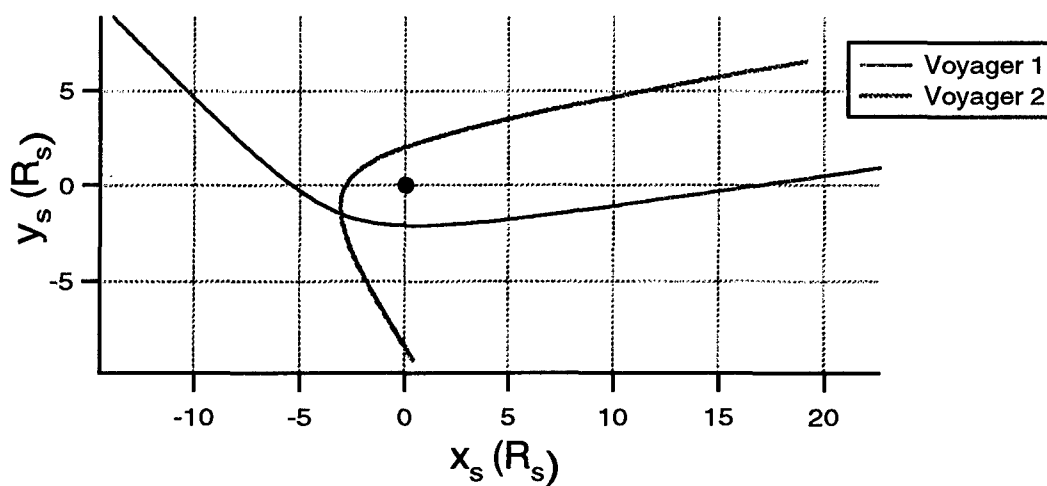


Figure 16. Projection of the Voyager 1 and Voyager 2 Trajectories in the x-y plane.

Since there are little data concerning the far night region where the tail dominates, it is impossible to see how well the magnetotail model compares with the actual conditions in the Saturnian neighborhood. Comparisons of V1 and V2 magnetometer data with the above model representation are still very useful in confirming the tail model by ensuring that inappropriate contributions have not been introduced. As can be seen in Figures 17 and 18, the theoretical results of the magnetotail-incorporated Saturnian model are very similar to the results obtained from the ME95 model in the regions where V1 and V2 flew by.

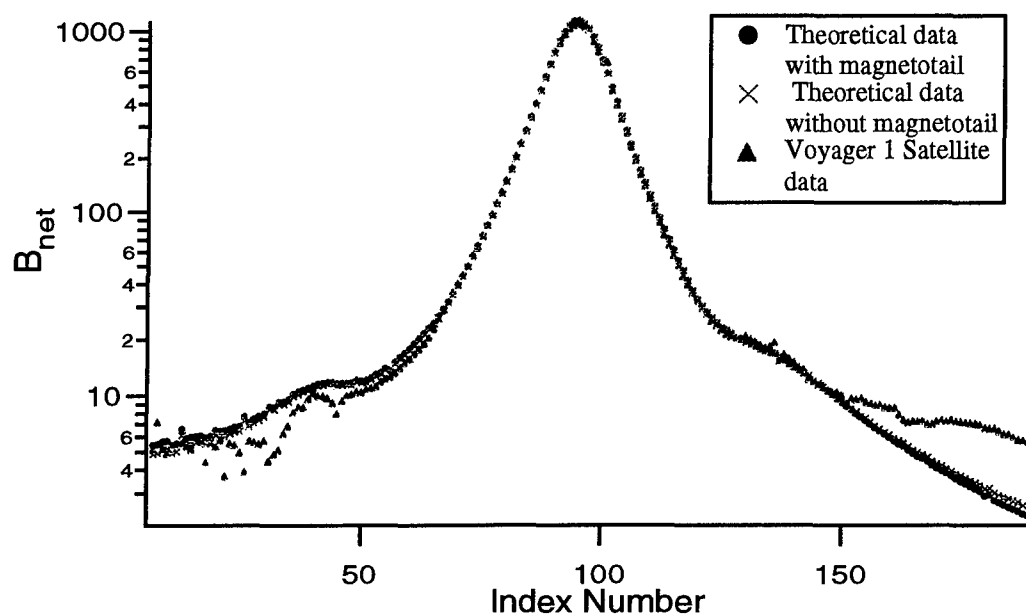


Figure 17. Comparison of net magnetic field vs. index number for Voyager 1. Index number represents times that the satellite measured data as it flew by the planet.

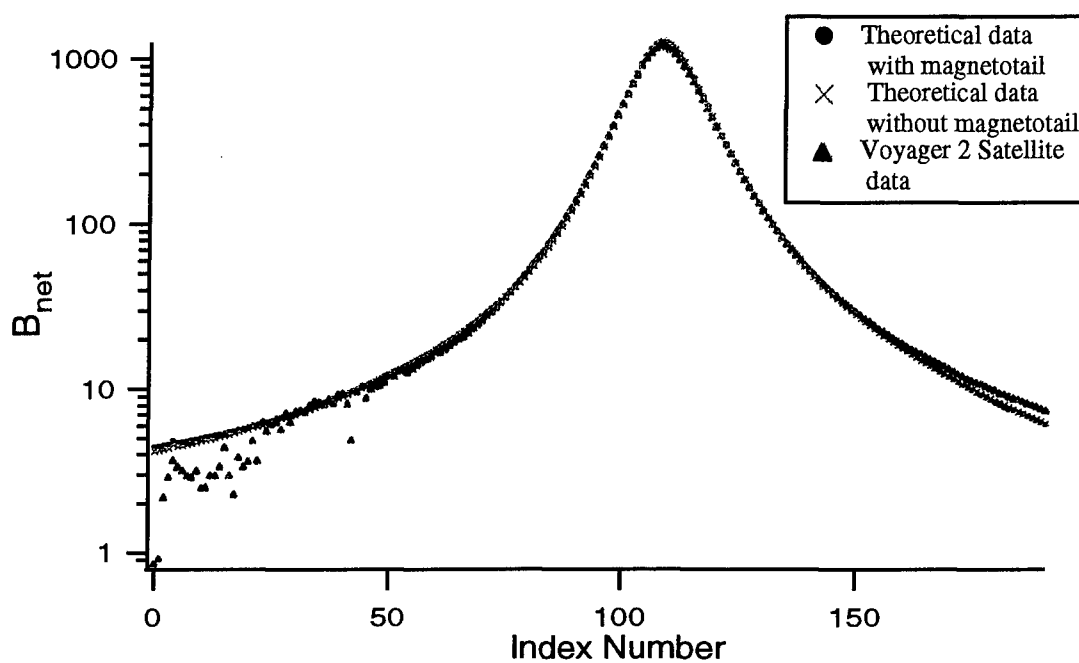


Figure 18. Comparison of net magnetic field vs. index number for Voyager 2.

Since the effects of the tail should be very small on the dayside of the magnetosphere, the results of Figures 17-18 coincide nicely with intuitive prediction of the magnetotail effects on the Saturnian magnetosphere.

Observation and comparison of the Earth's magnetosphere with Saturn's predict that a finite cross current structure sheet should be present in the night region of the Saturnian magnetosphere. Thus, the inclusion of a magnetotail to the Saturnian magnetosphere is necessary in order to have an accurate magnetosphere model in the night region. The lack of a magnetotail in the ME95 model severely limited the range of applicability to $x_s \approx -15 R_s$. The new model is predicted to be valid for observational purposes to $x_s > -120 R_s$. This will be extremely useful for the Cassini project since the spacecraft will perform orbits about Saturn and collect large portions of data in the night region. Consequently, the model presented in this paper is the only one available for comparing magnetometer trends in the night region with magnetohydrodynamics.

To reflect the space environment during the Cassini spacecraft's arrival at Saturn, further refinements are necessary to the magnetosphere model. The Cassini space probe will arrive at Saturn in 2004 when the solar wind will be incident at an angle of approximately -18° relative to the magnetic equator [*Cassini Project*, 1994]. Consequently, a "tilted" magnetosphere model similar to the MEBS96 model is necessary for incorporation of the magnetotail model in order to simulate the conditions at Saturn when Cassini will arrive.

VI. Non-idealized (Tilted Model)

The contributions of the model previously discussed are idealized in the sense that they only account for a brief period of time during the Saturnian orbit around the sun (those times when the incident solar wind velocity is parallel to the magnetic equator). During this time, symmetry exists across the magnetic equator. In other words, the shapes of the magnetic field lines in the northern hemisphere are mirrored in the southern hemisphere. For the sake of visualization, the direction of the solar wind can be represented as a vector originating at the center of the Sun and ending at the center of Saturn. Thus, as Saturn orbits around the Sun, there exists an angle, λ_{sw} , between the solar wind vector and the magnetic equator. When Cassini arrives, the orientation of the solar wind with the magnetic equator will be similar to the simplified diagram of Figure 19.

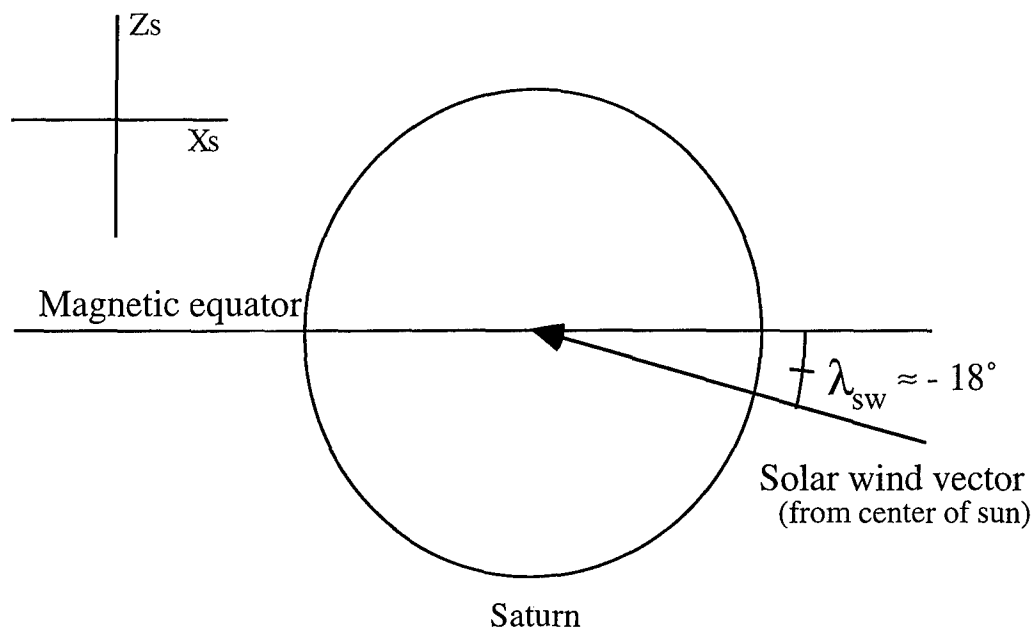


Figure 19. Simplified representation of Saturn showing the solar wind vector orientation with respect to the magnetic equator. A set of axes in the upper left corner show the orientation of the planetary magnetic field.

The Figure is shown in the Saturnian magnetic field coordinate system where the z axis, z_s , is parallel to the dipole moment. Thus, the x axis, x_s , is parallel to the magnetic equator. In the Saturnian magnetic coordinate system, the orientation of the magnetic equator remains in the x - y plane and the solar wind vector orientation with respect to the magnetic equator is predicted to vary from $\lambda_{sw} = +26.7^\circ$ to $\lambda_{sw} = -26.7^\circ$ over a given Saturnian orbit around the Sun.

It is assumed that varying λ_{sw} has no effect on the internal contributions of the Saturnian magnetic field. Consequently, the values of \vec{B}_D and \vec{B}_{RC} remain the same as they were in the idealized model. The non zero λ_{sw} , however, results in a break in the north-south mirror symmetry of the magnetopause. Subsequently, the values of \vec{B}_{SC} are adjusted in accordance with the chosen value of λ_{sw} .

A. Effects of the non-zero λ_{sw} on the magnetotail

A basic rotation of the coordinate transformation in the x-z plane of the magnetotail coordinate system about the y axis is used to account for non-zero λ_{sw} in the magnetotail. (It should be noted that the x-z plane of the magnetotail coordinate system and the x-z plane of the Saturnian magnetic equator coordinate system are parallel). A given point in the magnetosphere is converted to a magnetotail coordinate system via a rotation about the y-axis as follows

$$\begin{aligned} X_{\text{tilted}} &= \cos(\lambda_{sw}) X_{\text{original}} + \sin(\lambda_{sw}) Z_{\text{original}} \\ \text{and} \\ Z_{\text{tilted}} &= -\sin(\lambda_{sw}) X_{\text{original}} + \cos(\lambda_{sw}) Z_{\text{original}}. \end{aligned} \quad (37)$$

Thus, the final complete spatial coordinate transformation between the Saturnian magnetotail system and the Beard Earth magnetotail can be represented as

$$\begin{bmatrix} X_{\text{Saturn}} \\ Y_{\text{Saturn}} \\ Z_{\text{Saturn}} \end{bmatrix} = \begin{bmatrix} \cos(\lambda_{sw}) & 0 & \frac{\sin(\lambda_{sw})}{2.4} \\ 0 & \frac{1}{3.029} & 0 \\ -\sin(\lambda_{sw}) & 0 & \frac{\cos(\lambda_{sw})}{2.4} \end{bmatrix} \begin{bmatrix} X_{\text{Earth}} \\ Y_{\text{Earth}} \\ Z_{\text{Earth}} \end{bmatrix}. \quad (38)$$

Note that for $\lambda_{sw} = 0$, equation (31) is obtained.

After the spatial coordinates are transformed and the magnetic field is calculated, the magnetic field components must be converted so that the magnetic field vectors are represented in the Saturn coordinate system as opposed to the magnetotail coordinate system. This is obtained by applying a rotation on the magnetic field vectors in the x-z plane as follows

$$\begin{aligned} \vec{B}_{X \text{ Saturn}} &= \cos(\lambda_{sw}) \vec{B}_{X \text{ magnetotail}} - \sin(\lambda_{sw}) \vec{B}_{Z \text{ magnetotail}} \\ \text{and} \\ \vec{B}_{Z \text{ Saturn}} &= \sin(\lambda_{sw}) \vec{B}_{X \text{ magnetotail}} + \cos(\lambda_{sw}) \vec{B}_{Z \text{ magnetotail}} \end{aligned} \quad (39)$$

A graph of the noon-midnight meridian plot of the magnetic field due to just the magnetotail contribution for Saturn at a $\lambda_{\text{SW}} = -20^\circ$ is shown in Figure 20.

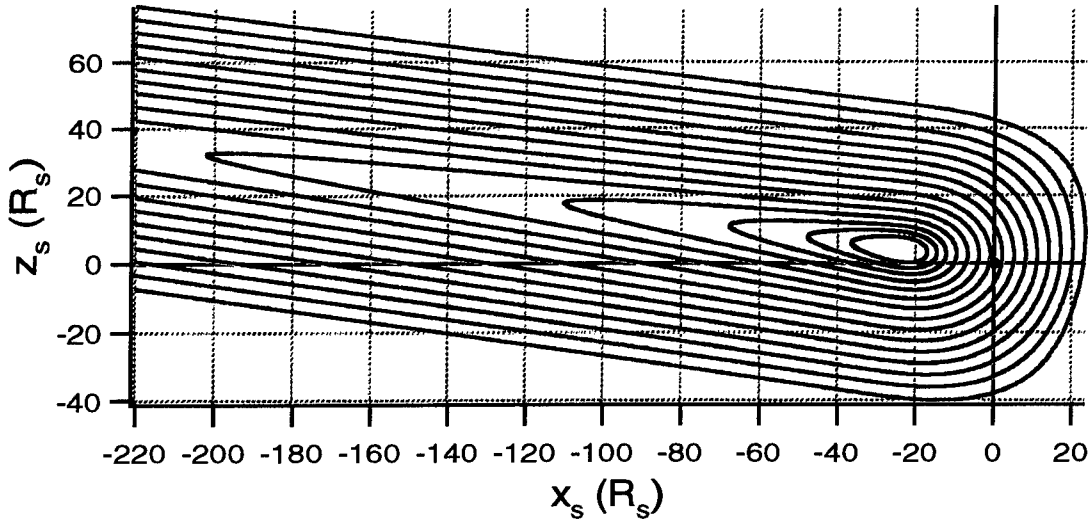


Figure 20. Noon-midnight meridian field tracing of the magnetotail magnetic field for Saturn for $\lambda_{\text{SW}} = -20^\circ$. The coordinate system is centered on the planet with the positive x coordinate pointing towards the sun and the z axis aligned with the magnetic dipole axis of Saturn.

B. Effects of the non-zero λ_{SW} on the magnetopause surface current elements

From the geometry of the solar wind vector in relation to the magnetic equator, the generalized solar wind velocity vector is found to be [Beard, 1960]:

$$\begin{aligned}
 -\vec{v}_{\text{SW}} = & [\cos(\theta)\sin(\lambda_{\text{SW}}) + \cos(\phi)\sin(\theta)\cos(\lambda_{\text{SW}})]\hat{r} \\
 & + [\cos(\phi)\cos(\theta)\cos(\lambda_{\text{SW}}) - \sin(\theta)\sin(\lambda_{\text{SW}})]\hat{\theta} \\
 & - [\sin(\phi)\cos(\lambda_{\text{SW}})]\hat{\phi}
 \end{aligned} \tag{40}$$

As a result of equation (40), the pressure balance consequence, $|\hat{n}_s \cdot \hat{v}_s| = |\hat{n}_s \times \vec{B}|$, is generalized to account for non-zero values of λ_{SW} .

Although the necessary adjustments to generalize the idealized model to account for non-zero λ_{SW} are small, the changes to the magnetopause shape are significant, as can be seen by Figure 21, where $\lambda_{\text{SW}} = -20^\circ$.

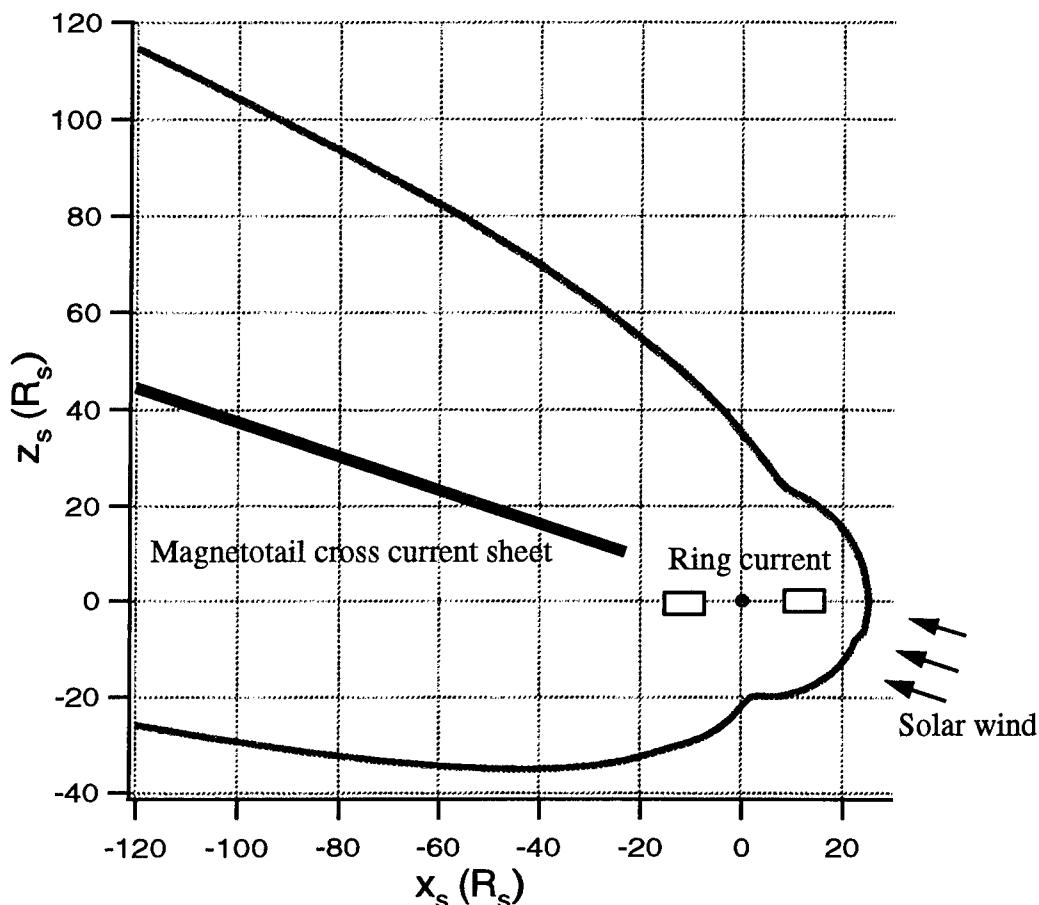


Figure 21. Trace of the Saturnian magnetopause in the noon-midnight meridian plane for a $\lambda_{SW} = -20^\circ$. The location of the magnetotail cross current sheet shown in red and the intersection of the azimuthal ring current with the plane are superimposed on the Figure for spatial reference.

The breaking of the north-south symmetry is apparent when comparing Figure 21 with Figure 12. The number of grid point locations which must be explored are doubled as a result. This also doubles the possibility of overlooking non-convergent behavior during the iterative process. Another difference is that the location of the sub-solar point becomes questionable in the "tilted" model. Since the subsolar point is used for normalization purposes, inaccurately locating the subsolar point can have negative, non-convergent effects on the whole model. Accurate intuition and observations of the developer become imperative to obtaining self-consistent results as a consequence of these difficulties.

VII. Discussion and Conclusion

The result of this research is a three-dimensional approximated self-consistent global magnetospheric model of Saturn with its associated magnetopause. The range of validity of this model is significantly extended on the night side of Saturn relative to the ME95 model due to the incorporation of a magnetotail into the global magnetosphere. The model presented in this paper obeys the requirements of magnetohydrodynamics and is not restricted to locations where satellite data was obtained, unlike empirically fit models. There is no direct way to confirm the validity of the incorporation of the magnetotail model into the Saturnian magnetosphere; however, a comparison of the model to available V1 and V2 data confirms that no un-physical deviations have been introduced as a consequence of the magnetotail incorporation.

Further modifications can be made to the models presented above. The interaction of the solar wind and inclusion of a magnetotail disrupts the axial symmetry of the ring current. Thus, a non-axisymmetric ring current model is an inevitable adjustment for complete accuracy of the ultimate model. A refinement is also desirable for the shape of the ring current cross section, since the sharp boundaries of the model cause anomalous magnetic field elements in the numerical integration.

The Cassini spacecraft will arrive at Saturn when $\lambda_{SW} \approx -18.0^\circ$ and will perform *in situ* orbits around Saturn until 2008 when $\lambda_{SW} \approx -4.0^\circ$ [Cassini Project, 1994]. Thus, production of self-consistent "tilted" Saturnian magnetospheric models at various intermediary angles ($\lambda_{SW} = -15.0^\circ, -10.0^\circ$ and -5.0°) will be useful for complete analysis of the Cassini project. Results for other desired λ_{SW} can then be obtained via interpolation among the future models. These models can then be used to understand the magnetometer data and plasma observations obtained by the Cassini spacecraft. When a sufficient amount of magnetometer data are collected in the night region of Saturn by Cassini, the magnetotail analogy will no longer be necessary. Refined parameters for a Saturnian magnetotail model can then be obtained by directly fitting to the Cassini magnetometer data. In the meantime, the results presented in this paper provide the most sophisticated global Saturnian magnetospheric model available to date.

Bibliography:

Acuna, M. H. and N. F. Ness, The Magnetic Field of Saturn: Pioneer Observations, *Science*, **207**, 444-446, 1980.

Beard, D. B., The Interaction of the Terrestrial Magnetic Field with the Solar Corpuscular Radiation, *Journal of Geophysical Research*, **65**, 3559, 1960.

Beard, D. B., The Magnetotail Magnetic Field, *Journal of Geophysical Research*, **84**, 2118-2124, 1979.

Behannon, K. W., Mapping of the earth's bow shock and magnetotail by Explorer 33, *Journal of Geophysical Research*, **73**, 907-930, 1968.

Cassini Project, Mission Plan, JPL D-5564, Rev. D, Jet Propul. Lab., Pasadena, California, 1994.

Connerney, J. E. P., M. H. Acuna, and N. F. Ness, Currents in Saturn's Magnetosphere, *Journal of Geophysical Research*, **88**, 8779-8789, 1983.

Engle, I. M. and D. B. Beard, Idealized Jovian Magnetosphere Shape and Field, *Journal of Geophysical Research*, **85**, 579-592, 1980.

Griffiths, D. J., *Introduction to Electrodynamics*, Simon & Schuster Co., 234-238, 1989.

Harris, E. G., On a Plasma Sheet Separating Regions of Oppositely Directed Magnetic Fields, *Nuovo Cimento*, **23**, 115-121, 1962.

Kivelson, M. G., Physics of Space Plasmas, in *Introduction to Space Physics*, edited by M. G. Kivelson and C. T. Russell, Cambridge University Press, Cambridge, 41-50, 1995.

Lepping, R. P., L. F. Burlaga, L. W. Klein, J. M. Jensen, and C. C. Goodrich, Observations of the magnetic field and plasma flow in Jupiter's Magnetosheath, *Journal of Geophysical Research*, **86**, 8141, 1981.

Maurice, S. and I. M. Engle, Idealized Saturn Magnetosphere Shape and Field, *Journal of Geophysical Research*, **100**, 17143-17151, 1995.

Maurice, S., I. M. Engle, M. Blanc, and M. Skubis, The Geometry of Saturn's Magnetopause, *Journal of Geophysical Research*, **101**, 27053-27059, 1996.

Mead, G. D. and D.B. Beard, Shape of the Geomagnetic Field Solar Wind Boundary, *Journal of Geophysical Research*, **69**, 1169, 1964.

Ness, N. F., M. H. Acuna, R.P. Lepping, J. E. P. Connerney, K. W. Behannon, L. F. Burlaga, Magnetic Field Studies by Voyager 1: Preliminary Results at Saturn, *Science*, **212**, 213, 1981.

Smith E. J., L. Davis, D. E. Jones, P. J. Coleman, D. S. Colburn, P. Dyal, C. P. Sonett, Saturn's Magnetosphere and its Interaction with the Solar Wind, *Journal of Geophysical Research*, **85**, 5655-5673, 1980.

Appendix A - Derivation of the equation for a pure dipole field

Deriving the general equation for a pure dipole starts from the definition of the magnetic vector potential,

$$\vec{A} = \frac{\mu_0}{4\pi} \int \frac{\vec{J}}{|\vec{r} - \vec{r}'|} dV. \quad (1)$$

The function $\frac{1}{|\vec{r} - \vec{r}'|}$ can be represented as an expanded power series,

$$\frac{1}{|\vec{r} - \vec{r}'|} = \frac{1}{r} \sum_{n=0}^{\infty} \left(\frac{r'}{r}\right)^n P_n(\cos \theta) \quad (2)$$

where $P_n(\cos \theta)$ are the Legendre polynomials. By substituting equation (2) back into the vector potential, equation (1), and expanding out to $n=2$ the following result is obtained

$$\vec{A} \approx \vec{J} \frac{\mu_0}{4\pi} \left[\frac{1}{r} \int_{CL} dV + \frac{1}{r^2} \int_{CL} (r' \cos \theta dV) + \frac{1}{r^3} \int_{CL} r'^2 \left(\frac{3}{2} \cos^2 \theta - \frac{1}{2} \right) dV \right]$$

where $\int_{CL} dV$ is a closed loop integral and consequently zero since it is the displacement of a vector around a closed loop. Consequently, this term, called the monopole, is always zero. This result coincides nicely with the physical observation that a magnetic monopole does not exist in nature. The second term, however, is the dipole and is the one relevant to the Saturnian model:

$$\vec{A}_{\text{dipole}} = \vec{J} \frac{\mu_0}{4\pi} \left[\frac{1}{r^2} \int_{CL} (r' \cos \theta dV) \right]. \quad (3)$$

It can be shown, using vector calculus, that the integral in equation (3) can be represented in a more useful form

$$\int_{CL} (r' \cos \theta \, dV) = -\frac{1}{2} \hat{r} \times \int_{CL} (r' \times dV) . \quad (4)$$

Therefore, by substituting equation (4) into equation (3) the following result is obtained

$$\vec{A}_{\text{dipole}} = \vec{J} \frac{\mu_0}{4\pi r^2} \left[-\frac{1}{2} \hat{r} \times \int_{CL} (r' \times dV) \right] = \frac{\mu_0}{4\pi r^2} (\vec{m} \times \hat{r}) \quad (5)$$

$$\text{where } \vec{m} = \frac{1}{2} \vec{J} \int_{CL} (r' \times dV) .$$

Equation (5) can be presented in a more simple form:

$$\vec{A}_{\text{dipole}} = \frac{\mu_0}{4\pi r^2} [\vec{m}(\sin \theta)] \hat{\phi} . \quad (6)$$

By assuming that the dipole magnetic vector potential above is the highest order of the approximation magnetic dipole, the formula for a pure magnetic dipole can be obtained by taking the curl of (6).

$$\vec{B}_{\text{dipole}} = \vec{\nabla} \times \vec{A}_{\text{dipole}} = \frac{\mu_0}{4\pi r^3} m [(2\cos \theta) \hat{r} + (\sin \theta) \hat{\theta}]$$

This is the resulting dipole equation that is applied to the Saturnian magnetosphere.

Appendix B - Derivation of the equation for magnetic pressure

Deriving the equation for magnetic pressure starts from the momentum equation of magnetohydrodynamics,

$$\frac{\partial(\rho_s \vec{u}_s)}{\partial t} + \vec{\nabla} \cdot (\rho_s \vec{u}_s \vec{u}_s) = -\vec{\nabla} p_s + q_s n_s \vec{E} + \vec{J}_s \times \vec{B} + \frac{p_s \vec{G}_g}{m_s} \quad (1)$$

This equation represents the relationship between the momentum and force of a fluid comprised of a particle, s , as determined from flux conservation. The first term on the right represents the pressure force due to spatial gradients in the pressure as momentum is transferred through the system. The second term represents the force due to the electric field which will be considered negligible. The third term represents the force exerted by the magnetic field. The fourth term represents gravitational and any other non-electrodynamics forces. The third term on the right of equation (1) can be expanded by solving Ampere's law for a non-time dependent electric field, $\vec{\nabla} \times \vec{B} = \mu_0 \vec{J}$, for \vec{J} and substituting it into $\vec{J}_s \times \vec{B}$:

$$\vec{J}_s \times \vec{B} = \left(\frac{\vec{\nabla} \times \vec{B}}{\mu_0} \right) \times \vec{B} = \frac{-\vec{\nabla}(B^2)}{2\mu_0} + (\vec{B} \cdot \vec{\nabla}) \frac{\vec{B}}{\mu_0} \quad (2)$$

Substituting equation (2) into equation (1) and grouping the gradient terms together shows the following result for the momentum equation.

$$\begin{aligned} \frac{\partial(\rho_s \vec{u}_s)}{\partial t} + \vec{\nabla} \cdot (\rho_s \vec{u}_s \vec{u}_s) = \\ -\vec{\nabla} \left(\frac{B^2}{2\mu_0} + p_s \right) + q_s n_s \vec{E} + (\vec{B} \cdot \vec{\nabla}) \frac{\vec{B}}{\mu_0} + \frac{p_s \vec{G}_g}{m_s} \end{aligned} \quad (3)$$

Note that the first term on the right of equation (3) represents the pressure relationship of the momentum equation. Consequently, the magnetic contribution to the pressure of the system is $P_B = \frac{B^2}{2\mu_0}$.

Appendix C - The non-zero coefficients, $G_{\lambda,m}$, of Φ_{MP} for $\lambda_{sw} = 0.0^\circ$

| $G_{\lambda,m}$ | Value | $G_{\lambda,m}$ | Value |
|-----------------|---------------------------|-----------------|---------------------------|
| $G_{1,0}$ | $+7.175 \times 10^{-01}$ | $G_{7,6}$ | $- 2.556 \times 10^{-03}$ |
| $G_{2,1}$ | $+3.573 \times 10^{-01}$ | $G_{8,1}$ | $- 4.765 \times 10^{-05}$ |
| $G_{3,0}$ | $+2.951 \times 10^{-02}$ | $G_{8,3}$ | $+6.875 \times 10^{-03}$ |
| $G_{3,2}$ | $+5.066 \times 10^{-02}$ | $G_{8,5}$ | $+4.675 \times 10^{-04}$ |
| $G_{4,1}$ | $+7.377 \times 10^{-02}$ | $G_{8,7}$ | $- 9.949 \times 10^{-04}$ |
| $G_{4,3}$ | $+5.710 \times 10^{-03}$ | $G_{9,0}$ | $- 8.447 \times 10^{-03}$ |
| $G_{5,0}$ | $+3.815 \times 10^{-04}$ | $G_{9,2}$ | $+2.169 \times 10^{-05}$ |
| $G_{5,2}$ | $+3.272 \times 10^{-02}$ | $G_{9,4}$ | $+1.052 \times 10^{-03}$ |
| $G_{5,4}$ | $+2.113 \times 10^{-03}$ | $G_{9,6}$ | $- 5.204 \times 10^{-05}$ |
| $G_{6,1}$ | $+2.530 \times 10^{-02}$ | $G_{9,8}$ | $- 1.558 \times 10^{-04}$ |
| $G_{6,3}$ | $+9.145 \times 10^{-03}$ | $G_{10,1}$ | $- 1.003 \times 10^{-04}$ |
| $G_{6,5}$ | $- 1.921 \times 10^{-03}$ | $G_{10,3}$ | $+2.567 \times 10^{-04}$ |
| $G_{7,0}$ | $- 9.965 \times 10^{-03}$ | $G_{10,5}$ | $- 4.188 \times 10^{-04}$ |
| $G_{7,2}$ | $+1.785 \times 10^{-02}$ | $G_{10,7}$ | $- 1.616 \times 10^{-04}$ |
| $G_{7,4}$ | $+1.973 \times 10^{-03}$ | $G_{10,9}$ | $- 2.650 \times 10^{-07}$ |